NOAA Technical Report NESDIS 146

doi:10.7289/V52B8W0Z

Report for
Dedicated JPSS VIIRS Ocean Color Calibration/Validation Cruise

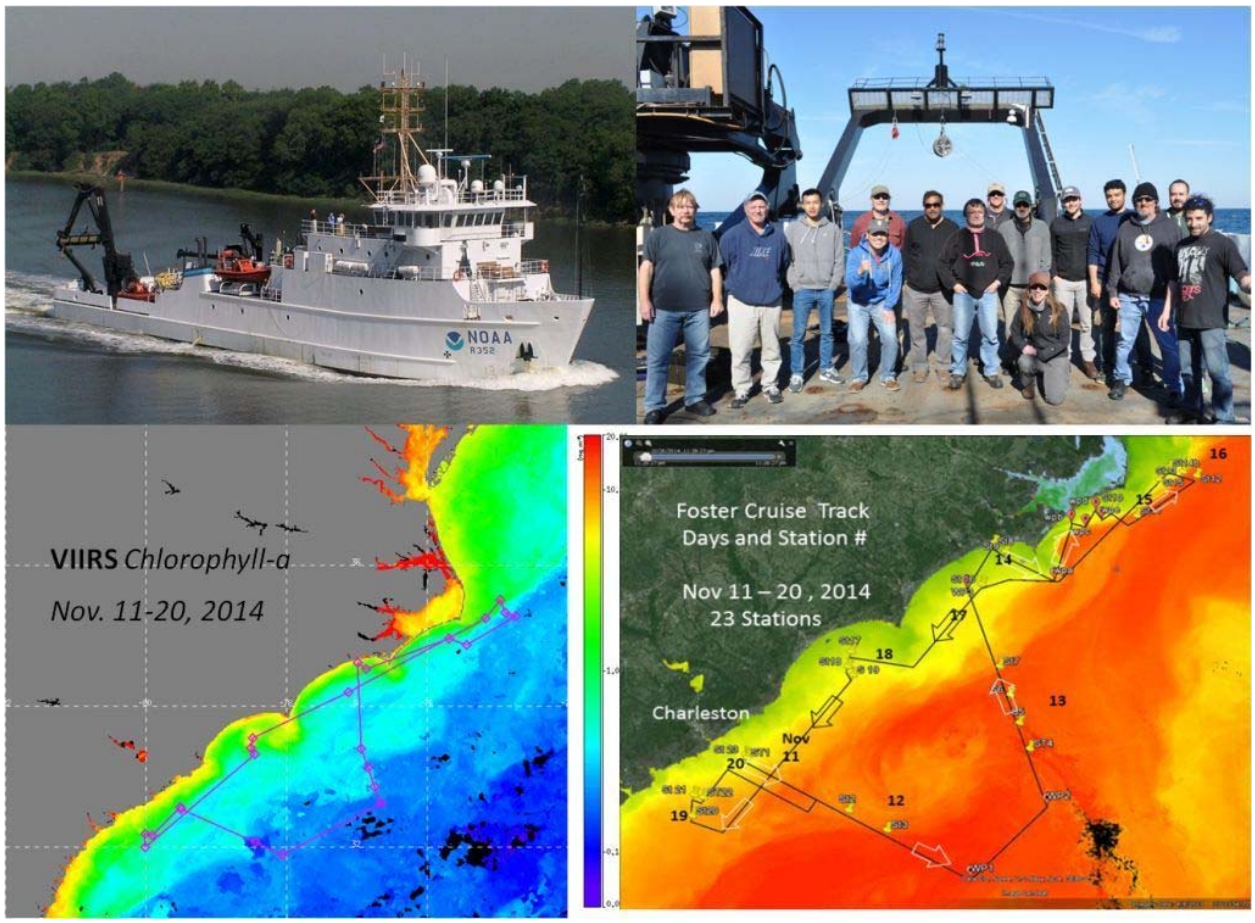

Washington, D.C.
September 2015

U.S. DEPARTMENT OF COMMERCE
National Oceanic and Atmospheric Administration
National Environmental Satellite, Data, and Information Service

NOAA TECHNICAL REPORTS
National Environmental Satellite, Data, and Information Service

The National Environmental Satellite, Data, and Information Service (NESDIS) manages the Nation's civil Earth-observing satellite systems, as well as global national data bases for meteorology, oceanography, geophysics, and solar-terrestrial sciences. From these sources, it develops and disseminates environmental data and information products critical to the protection of life and property, national defense, the national economy, energy development and distribution, global food supplies, and the development of natural resources.

Publication in the NOAA Technical Report series does not preclude later publication in scientific journals in expanded or modified form. The NESDIS series of NOAA Technical Reports is a continuation of the former NESS and EDIS series of NOAA Technical Reports and the NESC and EDS series of Environmental Science Services Administration (ESSA) Technical Reports.

Copies of earlier reports may be available by contacting NESDIS Chief of Staff, NOAA/ NESDIS, 1335 East-West Highway, SSMC1, Silver Spring, MD 20910, (301) 713-3578.

*Cover image: Clockwise from top left: NOAA Ship *Nancy Foster*; cruise science participants; cruise track overlaid onto VIIRS Naval Research Laboratory (NRL) satellite image of sea surface temperature; cruise track overlaid onto VIIRS satellite image of chlorophyll-a concentration (both satellite images are time-binned 11-20 November 2014, the time interval of the cruise). See Figs. 1 and 2 for colorscales and more details.

NOAA Technical Report NESDIS 146

doi:10.7289/V52B8W0Z

Report for Dedicated JPSS VIIRS Ocean Color Calibration/Validation Cruise

Contributing authors by group:

Michael Ondrusek[1], Eric Stengel[1], Veronica P. Lance[1,2] and Menghua Wang[1]
[1]NOAA/NESDIS Center for Satellite Applications and Research (STAR), 5830 University Research Court, College Park, MD 20740, USA
[2]Global Science and Technology, Inc., 7855 Walker Drive, Suite 200, Greenbelt, MD 20770, USA

Kenneth J. Voss
Department of Physics, University of Miami, Knight Physics Building, Coral Gables, FL 33124, USA

Giuseppe Zibordi and Marco Talone
Joint Research Centre of the European Commission, Institute for Environment and Sustainability, Ispra, Italy

Zhongping Lee, Jianwei Wei and Junfang Lin
School for the Environment, University of Massachusetts Boston, 100 Morrissey Blvd, Boston, MA 02125, USA

Chuanmin Hu, David English, Charles Kovach and Jennifer Cannizzaro.
College of Marine Science, University of South Florida, 140 7th Avenue South, St. Petersburg, FL 33701, USA

Alex Gilerson, Sam Ahmed, Amir Ibrahim, Ahmed El-Habashi and Robert Foster
City College of New York of the City University of New York, 160 Convent Ave, New York, NY 10031, USA

Robert Arnone[3], Ryan Vandermeulen[3], Sherwin Ladner[4] and Wesley Goode[4]
[3]University of Southern Mississippi, Stennis Space Center, MS 39529, USA
[4]Naval Research laboratory, Stennis Space Center, MS 39529, USA

Joaquim I. Goes, Helga do Rosario Gomes, Alex Chekalyuk and Kali McKee
Lamont Doherty Earth Observatory at Columbia University, 61 Route 9W, Palisades, NY, 10964, USA

Scott Freeman[5,6] and Aimee Neeley[5,6]
[5]NASA Goddard Splace Flight Center 8800 Greenbelt Rd, Greenbelt, MD 20770, USA
[6]Science Systems and Applications, Inc, 10210 Greenbelt Road, Suite 600, Lanham, Maryland 20706, USA

B. Carol Johnson
National Institute of Standards and Technology, Physical Measurement Laboratory,100 Bureau Drive, Stop 8441, Gaithersburg, MD 20899-8441, USA

Edited by Veronica P. Lance[1,2]
NOAA/NESDIS Center for Satellite Applications and Research (STAR), 5830 University Research Court, College Park, MD 20740, USA
[2]Global Science and Technology, Inc., 7855 Walker Drive, Suite 200, Greenbelt, MD 20770, USA

Corresponding author: veronica.lance@noaa.gov

Washington, D.C.
September 2015

U.S. DEPARTMENT OF COMMERCE
Penny Pritzker, Secretary

National Oceanic and Atmospheric Administration
Dr. Kathryn Sullivan, Under Secretary of Commerce for Oceans and Atmosphere and NOAA Administrator

National Environmental Satellite, Data, and Information Service
Dr. Stephen Volz, Assistant Administrator

Contents

List of Figures

List of Tables

List of Equations

Preface

The NOAA/STAR ocean color team is focused on "end-to-end" production of high quality satellite ocean color products. In situ validation of satellite data is essential to produce the high quality, "fit for purpose" remotely sensed ocean color products that are required and expected by all NOAA line offices, as well as by external (both applied and research) users. In addition to serving the needs of its diverse users within the U.S., NOAA has an ever increasing role in supporting the international ocean color community and is actively engaged in the International Ocean-Colour Coordinating Group (IOCCG). The IOCCG, along with the Committee on Earth Observation Satellites (CEOS) Ocean Colour Radiometry Virtual Constellation (OCR-VC), is developing the International Network for Sensor Inter-comparison and Uncertainty assessment for Ocean Color Radiometry (INSITU-OCR). The INSITU-OCR has identified, amongst other issues, the crucial need for sustained in situ observations for product validation, with long-term measurement programs established and maintained beyond any individual mission.

NOAA has been actively working to support this goal for some time. Dennis Clark of NOAA, in collaboration with community colleagues, began collecting in situ observations for mission validation activities starting with the launch of the Coastal Zone Color Scanner (CZCS; the first ocean color sensor) in 1978. NOAA/STAR scientists continued in situ data collection activities throughout all other ocean color satellite missions. More recently, the NOAA/STAR Ocean Color Team has been making in situ validation measurements continually since the launch in fall 2011 of the Visible Infrared Imaging Radiometer Suite (VIIRS) aboard the Suomi National Polar-orbiting Partnership (SNPP) platform, part of the U.S. Joint Polar Satellite System (JPSS) program. NOAA ship time for the purpose of ocean color validation, however, had never been allocated until the cruise described herein.

As the institutional lead for this cruise, NOAA/STAR invited external collaborators based on scientific objectives and existing institutional collaborations. The invited collaborators are all acknowledged professionals in the ocean color remote sensing community. Most of the cruise principal investigators (PIs) are also PIs of the VIIRS Ocean Color Calibration and Validation (Cal/Val) team, including groups from Stennis Space Center/Naval Research Laboratory (SSC/NRL) and the University of Southern Mississippi (USM); City College of New York (CCNY); University of Massachusetts Boston (UMB); University of South Florida (USF); University of Miami (U. Miami); and, the National Institute of Standards and Technology (NIST). These Cal/Val PIs participated directly, sent qualified researchers from their labs/groups, or else contributed specific instruments or equipment. Some of the cruise PIs are not part of the NOAA VIIRS Ocean Color Cal/Val team but were chosen to complement and augment the strengths of the Cal/Val team participants. Outside investigator groups included NASA Goddard Space Flight Center (NASA/GSFC), Lamont-Doherty Earth Observatory at Columbia University (LDEO), and the Joint Research Centre of the European Commission (JRC).

This report documents the November 2014 cruise off the U.S. East Coast aboard the NOAA Ship *Nancy Foster*. This cruise was the first dedicated ocean color validation cruise to be supported by the NOAA Office of Marine and Air Operations (OMAO). A second OMAO-supported cruise aboard the *Nancy Foster* is being planned for late 2015. We at NOAA/STAR are looking forward to continuing dedicated ocean color validation cruises, supported by OMAO on NOAA vessels, on an annual basis in support of JPSS VIIRS on SNPP, J-1, J-2 and other forthcoming satellite ocean color missions from the U.S as well as other countries. We also look forward to working with the U.S. and the international ocean community for improving our understanding of global ocean optical, biological, and biogeochemical properties.

Menghua Wang
Chief, Marine Ecosystems & Climate Branch; VIIRS Ocean Color Cal/Val Team Lead
Paul DiGiacomo
Chief, Satellite Oceanography & Climatology Division; NOAA Rep. to the IOCCG; OCR-VC Co-Chair

NOAA Technical Report NESDIS 146
Report for
Dedicated JPSS VIIRS Ocean Color Calibration/Validation Cruise

1. Overview of Purpose, Project, Principal Investigators and Participants

The purpose of this cruise aboard the NOAA Ship *Nancy Foster* was to collect in situ optical and ancillary data for validation of JPSS VIIRS satellite ocean color radiometry and derived products [*Wang et al.*, 2013; *Wang et al.*, 2014]. Specific objectives are detailed below in Section 3. The project interval was 9 to 22 November 2014. This 14-day interval included 10 days at sea (including transits), 2 staging days, 1 de-staging day and 1 day crew rest. Days at sea were 11 to 20 November 2014. Ship time aboard the NOAA Ship *Nancy Foster* (http://www.moc.noaa.gov/nf/) was funded through an allocation by the NOAA Office of Marine and Aviation Operations (OMAO). Ten investigator groups from 11 institutions participated in the cruise. Table 1 lists the principal investigators of the research groups, their institutions and the abbreviation used for the research group throughout this document. Fifteen scientists (maximum berthing allowance; see Table 2) sailed and conducted measurements with the support of officers and crew aboard the *Nancy Foster*. The Chief Scientist was Michael Ondrusek of NOAA/STAR. The cruise departed from and returned to Charleston, SC, USA, the Foster's home port. The primary area of operations was the Western Atlantic along the U.S. Mid- and Southeastern Coast, including cross-shelf, Gulf Stream and blue waters. The cruise track was optimized to accommodate sampling transient features present in the region while respecting weather conditions during the time of the cruise (Fig. 1). The cruise transected over 1800 km and occupied 23 stations for collection of underway and profile ocean color measurements during the 10-day duration. As expected in November in the Gulf Stream region, the weather conditions changed daily to represent a wide variety of atmospheric conditions, from cloudy to clear days. On several days, in situ measurements coincided with cloud free VIIRS satellite overpasses, enabling "match ups" for the purpose of ocean color validation. In addition, laboratory calibrations were conducted in collaboration with NIST at the STAR facility in College Park, Maryland both before and after the cruise. The laboratory calibrations used NIST traceable lamps. NIST also developed a reference plaque to be used on board for an instrument intercomparison exercise.

Table 1. Principal investigators (PIs), participating institutions and institution abbreviations.

PI Name (Last, First)	Participating Institutions	Research Group Abbreviation
Ondrusek, Michael*	NOAA/NESDIS Center for Satellite Applications and Research	NOAA/STAR
Ahmed, Sam	City College of New York	CCNY
Arnone, Robert	University of Southern Mississippi (USM) and Naval Research Center (NRL)	Stennis
Freeman, Scott	NASA Goddard Space Flight Center	NASA/GSFC
Gilerson, Alex	City College of New York	CCNY
Goes, Joaquim	Lamont-Doherty Earth Observatory at Columbia University	LDEO
Hu, Chuanmin	University of South Florida	USF
Johnson, B. Carol	National Institute of Standards and Technology	NIST
Lee, ZhongPing	University of Massachusetts, Boston	UMB
Neeley, Aimee	NASA Goddard Space Flight Center	NASA/GSFC
Voss, Kenneth	University of Miami	U. Miami
Zibordi, Giuseppe	Joint Research Centre of the European Commission	JRC

*Chief Scientist

Table 2. List of science party personnel aboard the *Nancy Foster* (alphabetical order).

Name (Last, First)	Title	Research Group/Home Institution*
Arnone, Robert	Research Professor	Stennis/USM
Freeman, Scott	Staff Research Scientist	NASA/GSFC
Goes, Joaquim	Research Professor	LDEO
el Habashi, Ahmed	PhD Student	CCNY
Ibrahim, Amir	PhD Student	CCNY
Kovach, Charles	Researcher	USF
Lin, Junfang	Postdoctoral Researcher	UMB
Neeley, Aimee	Staff Research Scientist	NASA/GSFC
Ondrusek, Michael	Chief Scientist	NOAA/STAR
Goode, Wesley	Researcher	Stennis/NRL
Stengel, Eric	Researcher	NOAA/STAR
Talone, Marco	Researcher	JRC
Vandermeulen, Ryan	Remote Sensing Analyst	Stennis/USM
Wei, Jianwei	Postdoctoral Researcher	UMB
Zibordi, Giuseppe	Researcher	JRC

*See Table 1 for institution abbreviations.

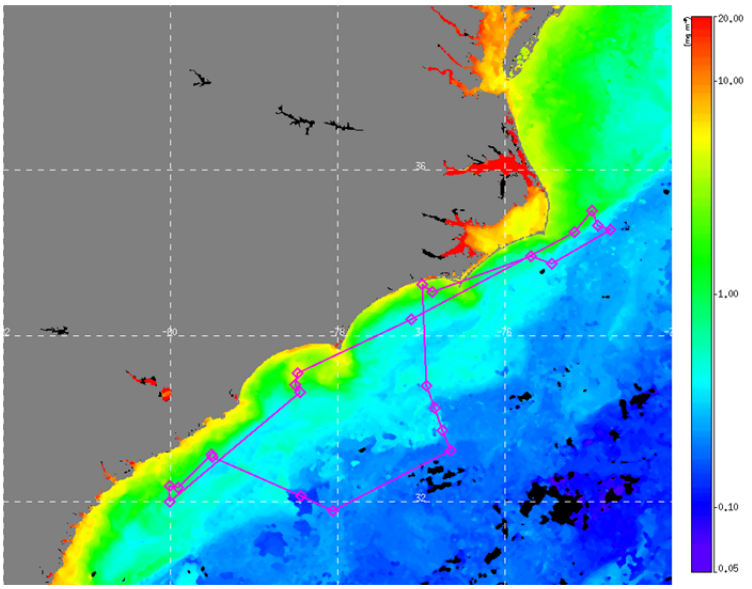

Figure 1. Cruise track of the *Nancy Foster* (project NF-14-09) overlaid onto an image of VIIRS chlorophyll *a* (Chl-*a*) binned for the time interval of 11–20 November 2014. The colorbar is a logarithmic scale from 0.05 mg m^{-3} to 20 mg m^{-3}.

The overall aim of this NOAA VIIRS Cal/Val Cruise is to validate VIIRS satellite ocean color data with the best quality in situ sensor radiances and derived products in multiple types of water masses (i.e., coastal, near-shore, cross-shelf, eddies, fronts, filaments, blue water) and to characterize uncertainties of these measurements. Data collected on this cruise will support many science and applied studies regarding satellite validation of remotely sensed ocean color, and of optical signatures of the highly variable Gulf Stream fronts. The cruise data collection will be deposited at NOAA

CoastWatch/OceanWatch and made available for convenient access to the ocean community and will be formally archived through NOAA/NESDIS/NCEI as required by NOAA.

2. Introduction

NESDIS has been providing ocean color validation and calibration support since the launch of the Coastal Zone Color Sensor (CZCS) [*Gordon et al.*, 1980; *Hovis et al.*, 1980] in the late 1970's. This includes cruises for the validation of satellite data and the development of the Marine Optical BuoY (MOBY) [*Clark et al.*, 1997] in the Sea-viewing Wide Field-of-view Sensor (SeaWiFS) era [*Gordon*, 2010]. Today, MOBY has become the primary vicarious calibration reference standard for all satellite ocean color sensors. This November 2014 VIIRS Calibration/Validation (Cal/Val) cruise is the first dedicated ocean color validation cruise aboard a NOAA research ship. The primary goals of the project include, in short, directly validating the VIIRS sensor, investigating uncertainties of in situ validation measurements and analyzing the capacity of VIIRS to study oceanic processes. To achieve these goals, twenty-three stations were occupied over 10 days along the southeast coast of the United States (Fig. 1). The stations were designed to allow investigators to make in situ measurements for validating the VIIRS performance in producing ocean color products, run simultaneous comparisons of the most widely utilized validation measurements and characterize oceanic processes in the study area. This design and the diligent work of the investigators and the crew of the *Nancy Foster*, enabled all planned goals to be achieved.

3. Cruise Objectives

The JPSS VIIRS-SNPP satellite ocean color program Cal/Val science plan calls for in situ observations for the purpose of developing and validating ocean color Environmental Data Records (EDR). The overall aim of this NOAA VIIRS Cal/Val Cruise is to validate VIIRS satellite ocean color data [*Wang et al.*, 2013; *Wang et al.*, 2014] with the best in situ sensor radiances and derived products in multiple types of water masses. Toward that aim, this NOAA cruise was dedicated to making shipboard observations of inherent and apparent optical properties in support of the three primary objectives: 1) VIIRS ocean color satellite validation observations; 2) characterization of differences among in situ ocean color measurements and 3) optical characterization of ocean variability (i.e., coastal, near-shore, cross-shelf, eddies, fronts, filaments, blue water). These three objectives are discussed further below.

1) Observe in situ properties for VIIRS ocean color satellite validation
Satellite validation methods "match up" satellite observations with in situ observations. The primary objective for this cruise was to collect high quality in situ measurements, including in-water, above water seaward and above water skyward, for the purpose of validating and evaluating the VIIRS performance for deriving ocean color products. Uncertainties associated with in situ observations are discussed in the second objective below.

2) Determine uncertainties associated with in situ ocean color measurements
The second cruise objective was to investigate the uncertainties of the in situ measurements that are used for calibration and validation of VIIRS ocean color products as described in objective 1 by documenting the differences observed under measurement conditions of repeatability and reproducibility [*GUM*, 1995]. For a recent description of how to apply uncertainty estimates to ocean color, see the review article by Johnson et al. [2014]. Uncertainties in products such as remote sensing reflectance that are derived from satellite ocean color data are associated with the determination of atmospheric correction [*Gordon and Wang*, 1994; *IOCCG*, 2010; *Wang*, 2007] and the bidirectional reflectance distribution function (BRDF) of the seawater. Products derived from the ocean color radiances, such as inherent optical properties (IOPs) and chlorophyll-a, are uncertain due to spatial and temporal variability as well as the veracity of the underlying model algorithms. The in situ measurements used in VIIRS product validation and measured in this cruise include both in-water and atmospheric parameters. The data sets assembled from this cruise will be analyzed to determine uncertainties, using the observed differences under conditions of

repeatability and reproducibility, and will be used in estimations of the uncertainty in the match ups of VIIRS and in situ data. The following approaches, which represent conditions of reproducibility, were used to quantify measurement differences associated with: a) replicate observations from multiple identical (same model) instruments deployed in parallel; b) observations of the same in situ parameters but using different types of instruments; c) different deployment protocols for sample collection; d) different post-processing methods for the in situ data; and e) spatial and temporal variability of the ocean waters.

a) *Differences associated with identical instruments and protocols* — Many investigators simultaneously deployed multiple instruments of the same make and model using identical collection protocols for in-water and above-water validation measurements.

b) *Differences from instrumentation* — Investigators deployed multiple instruments of different makes or models in parallel to measure the same in situ ocean color parameters. Collection protocols and processing are instrument-specific, therefore they are included as part of this analysis.

c) *Differences from sampling protocols* — Sampling protocols may differ among investigators and also among different types of instruments. Some investigators experimented with different sampling protocols using the same instrument. Where possible, the differences associated with collection protocols will be assessed (whether from the same or different types of instruments).

d) *Differences from post-processing methods* — Data sets from identical instruments and collection protocols (as discussed in Section 2a above) will be processed in multiple ways. First, data sets will be processed by individual investigators using their own preferred post-processing methods. Second, all data sets will be processed by one or more common post-processing methods.

e) *Differences in matchups due to spatial and temporal variability of the ocean waters* — From observation data collected at stations and from the underway seawater flow-through system, the spatial and temporal variability of the bio-optical properties water masses will be analyzed and compared with the nominal 750 m resolution of the VIIRS satellite-derived ocean color data. Changes in ocean color products occur with water mass movements. Temporal changes throughout the day and can occur within the nominal 750 m spatial resolution of VIIRS data, which can impact the matchup used for validation. Our objective is to define the coherent scales of these spatial and temporal changes for matchups between VIIRS and in situ measurements. This effort includes the evaluation of the VIIRS validation matchup uncertainty across the Gulf Stream fronts.

3) Characterize the optical properties of dynamic ocean processes

The third objective of this cruise is to optically characterize ocean variability related to dynamic processes in open and coastal waters for the purpose of exploring the utility of VIIRS ocean color products in identifying these dynamic regions from space. The Gulf Stream region represents a major ocean circulation structure, which is characterized by significant variability in optical and physical properties resulting from biological and physical processes as continental shelf waters interact with open waters to produce upwelling and downwelling regions, coastal fronts, advection and dispersion [*Arnone et al.*, 1990; *Dickey*, 1991]. The cruise data will be used to evaluate and demonstrate the ability of VIIRS ocean color products to differentiate the variations of spectral features produced by these physical and biological processes. For example, the optical properties of spectral absorption and backscattering coefficients may be associated with different phytoplankton functional groups. These phytoplankton functional groups could then be retrievable from VIIRS satellite data.

The three primary objectives described above encompass many specific questions that these cruise data will address, such as:

1. What differences among the in-water IOP or apparent optical property (AOP) observations are due to using different instruments and/or protocols?
2. How do above water measurements of water-leaving radiance ($L_w(\lambda)$) relate to in-water measurements of the normalized water-leaving radiance ($nL_w(\lambda)$)?
3. What are the differences in ocean color measurements between similar optical instruments at the same time and in the same waters?
4. How does the vertical structure of the IOPs and AOPs relate to the matchup of the VIIRS satellite products?
5. How does the VIIRS $nL_w(\lambda)$ matchup compare with the in situ measurements?
6. What is the sensitivity of the VIIRS-derived $nL_w(\lambda)$ spectra to the oceanic BRDF?
7. What is the spatial variability of IOP measurements observed in situ compared with those derived fromVIIRS?
8. How well can VIIRS characterize the gradient of changes in bio-optical properties across frontal boundaries?
9. How do changes in ocean color and IOPs across the Gulf Stream fronts relate to the biological functional groups and can VIIRS detect these changes?
10. How does chlorophyll-a determined from in situ fluorometers compare with the phytoplankton pigments determined by high performance liquid chromatography (HPLC)?
11. What is the sensitivity of chlorophyll-a estimates determined by in situ fluorometry to surface photoquenching?
12. Can water mass characterization representing different bio-physical processes be defined using VIIRS bio-optical products in a dynamic system such as the Gulf Stream?

4. Cruise Track, Sampling Strategies and Overall Conditions

The cruise departed Charleston, South Carolina on 11 November 2014 at 12:00 local EST (17:00 UTC) and proceeded eastward crossing the Gulf Stream on 12 November. The cruise track crossed back across the Gulf Stream to the northwest on 13 November and then headed northward along the coastal waters to offshore of Cape Hatteras on 16 November, where there was a crossing of the Gulf Stream front. The cruise turned southward along the coast waters to south of Charleston on 19 November and returned to Charleston on 20 November 2014.

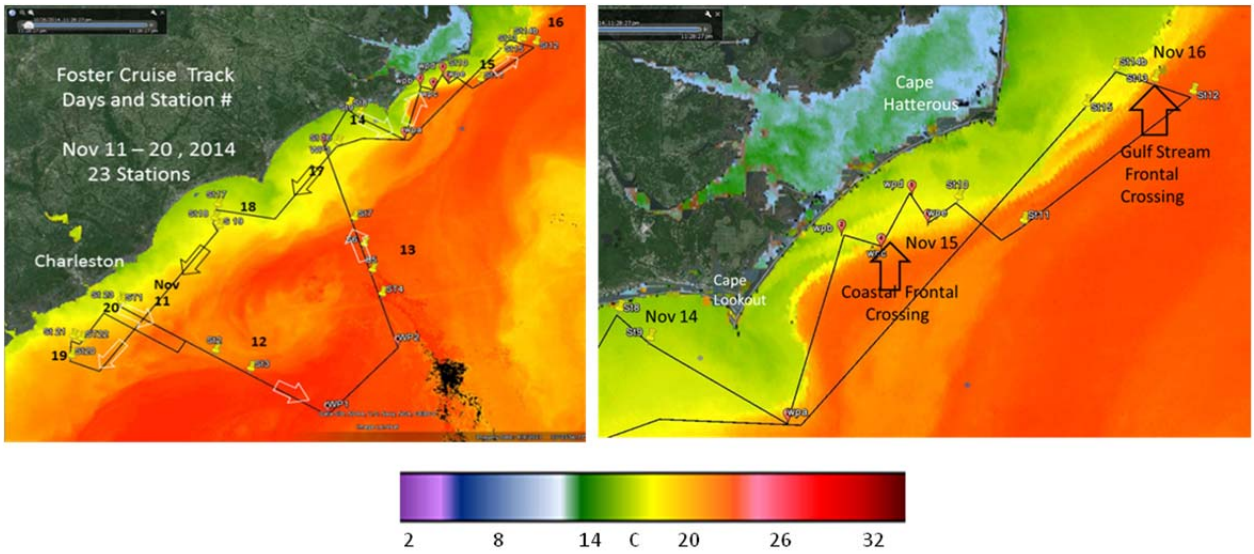

Figure 2. (Left panel) is the cruise track with station locations (1–23) and the date (November 11–21) with respect to the Gulf Stream illustrated here by the composite VIIRS sea surface temperature (SST). The colorbar scale is in units of °C. Black arrows are nighttime transects; white arrows are daytime, pins mark station locations, station numbers are indicated by S# in white and the dates of November are the black numbers. (Right panel) shows the Northern cruise track 14–16 November with the crossing of the Gulf Stream and coastal fronts.

Data collection was performed continuously throughout the cruise. Instruments were installed on the bow of the ship for making continuous observations from above water. Other instruments were installed on the ship's underway, surface sea water, flow-through system and were in operation continuously (day and night). Flow-through water was collected routinely for water sample analyses during nighttime transects. The cruise occupied shelf and coastal waters and had 4 major station transects into the Gulf Stream with stations spanning the Western front. Twenty-three discrete stations were conducted during daylight hours. These 23 stations began at 0800L and ended by 1600L (local, EST; add 5h for UTC). The stations were conducted daily, weather conditions permitting. Stations were planned to optimize cloud free conditions when they were available. Many of the station locations near the coast were selected based on predictions for cloud free conditions as the eastward passage of a cold front left the shelf waters cloud free.

<u>Gulf Stream sampling</u>
Stations:
12 Nov. – Stations 2 and 3 13 Nov. – Stations 4, 5, 6, 7
15 Nov. – Stations 10 and 11 16 Nov. – Stations 12, 13, 14, 15
<u>Underway:</u>
11-12 Nov. – Western front of Gulf Stream transiting in the Southeast direction
12-13 Nov. – Offshore Gulf Stream waters
19-20 Nov. – Two parallel crossings of Gulf Stream edges

<u>Shelf and coastal waters sampling</u>
Stations:
14 Nov. – Stations 8 and 9 15–18 Nov. – Stations 17, 18, 19
19 Nov. – Stations 20, 21, 22 20 Nov. – Station 23
Underway:
14–15 Nov. – Zigzag pattern through the shelf water fronts between stations 9 and 10
18–19 Nov. – Southern transects through shelf water fronts between stations 16 and 17

The weather conditions in November along the US East Coast resulted in several cloud-free days where matchup of VIIRS satellite and in situ data is possible. The weather changed during the cruise with the passage of several cold fronts on 13, 14 and 15 November, which brought strong winds reaching 30 knots, cloudy conditions and over 1.8 m seas. Partly overcast conditions followed on 16 and 17 November with increasing cloud cover and the passage of a second cold front. Cloud cover decreased and sky conditions began improving for validation observations on 18 November, with optimal sky conditions for validation occurring on the final days of the cruise, 19 and 20 November. A daily log can be found in Appendix B. Table A4 in Appendix A quantifies daily cloud coverage in percent of sky. Matchups between VIIRS satellite data and in situ station data were found for 4 separate days occurring at Stations 2, 3, 17, 18, 19, 20, 21, 22 and 23.

5. Overview of Observations

5.1. Introduction to Observations

Multiple optical instruments were assembled for this cruise to address the overall objectives and specific questions detailed above. In situ observations were made both on station and continuously from the underway bio-optical flow-through system along with logging traditional temperature, salinity and fluorescence by the ship's instruments. In the overview of instrumentation and observations that follows, optical instruments have been separated into two categories, "on station" and "continuous underway," and further categorized by mode of deployment and subdivided by parameters of interest. Note that some of the instruments were used for both on station and continuous underway sampling. Water samples were collected at stations at 3 discrete depths for later analyses and are further described in Section 5.4 following the instrumentation descriptions. The institutions responsible for operating equipment and collecting and analyzing samples are indicated. Readers should refer to the appropriate sub-section of Section 7 by each group for detailed reports on methods. A consolidated list of instrument identifying information is shown Table C2 in Appendix C. Also, see footnotes at the end of this section for brief notes regarding instrument calibrations. Calibration of radiometers is discussed in detail in Section 6.

Certain commercial equipment, instruments, or materials are identified in this report to foster understanding. Such identification does not imply recommendation or endorsement by the National Institute of Standards and Technology (NIST), nor does it imply that the materials or equipment identified are necessarily the best available for the purpose.

5.2. On Station Measurements

5.2.1. In-water profiling (observations with depth)

5.2.1.1. In-water profiling of ocean radiometry

These instruments were lowered through the water column and collected optical measurements that will be used for determining in-water AOPs; i.e., $nL_w(\lambda)$ data.

- HyperPro (Satlantic) – free-falling hyperspectral optical profiler (two profiling HyperPro instruments; NOAA/STAR and USF)[1].
- MicroPro (Satlantic) – free-falling multispectral optical profiler (JRC)[1].
- C-OPS (Biospherical Instruments, Inc.) – compact multispectral optical profiling system (NASA/GSFC)[1].

5.2.1.2. In-water profiling of IOPs

- ac-s plus ac-9 package (WET Labs) – in situ spectrophotometers[2] deployed as a package (the ac-9 was equipped with 0.22 µm particle filters on the intakes, the ac-s was unfiltered,) along with a ECO BB9 backscattering sensor and a VSF-9 volume scattering function sensor, both at nine

wavelengths (WET Labs), and additionally, an SBE 49 (SeaBird) for measuring conductivity (salinity), temperature and pressure (depth) nominally called a "CTD" (NASA/GSFC)
- Two ac-s (WET Labs) – in situ spectrophotometers, one equipped with a 0.22 μm particle filter on the intake, the other not, to discriminate between total absorption and chromophoric dissolved organic matter (CDOM) absorption with high spectral resolution[2] deployed as a package with BB7FL2 (WET Labs) which measures backscatter at seven channels and fluorescence at two channels (UMB)
- ECO Puck Triplet fluorometer (WET Labs) – chlorophyll, CDOM, and phycoerythrin (deployed with NOAA/STAR HyperPro profiling radiometer)
- ECO Puck Triplet scatterometer (WET Labs) – scattering at 3 wavelengths (443 nm, 550 nm and 860 nm; deployed with NOAA/STAR HyperPro profiling radiometer).
- ECO Puck Triplet fluorometer (WET Labs) – chlorophyll, CDOM, and scattering at 660nm (deployed with USF HyperPro profiling radiometer)
- SeaBird fluorometer (SeaBird) – chlorophyll fluorometer (ship's rosette package)

5.2.1.3. In-water profiling of other parameters

These parameters were observed by the standard instrumentation on the ship's CTD-rosette package.
- Salinity
- Temperature
- Dissolved O_2

5.2.2. Surface floating radiometry

These instruments were floated at the ocean surface during stations. Some of these packages also include sky-viewing components necessary for calculating final ocean color parameters.
- HyperTSRB (Satlantic) – hyperspectral radiometer configured to float on the sea surface (Stennis)[1]
- SBA [*Lee et al.*, 2013] – Sky- Blocking Apparatus (SBA) radiometer package composed of one HyperOCR (Satlantic); hyperspectral radiance sensor and one HyperOCI (Satlantic) hyperspectral irradiance sensor (UMB)
- NURADS [*Voss and Chapin*, 2005] – Upwelling Radiance Distribution Camera System (U. Miami).

5.2.3. Above water observations of ocean radiometry

These instruments measured the remote sensing reflectance (R_{rs}) from the vantage point of above the sea surface and looking down into the ocean. A blue glass tile with roughened surface mounted on a black plastic surface was provided by NIST as a test target. Gray plaques were also used as references.
- Analytical Spectral Device ASD (PANalytical) – spectrometer (five instruments; CCNY, Stennis/NRL, NOAA/STAR, USF, Stennis/USM)
- GER (Spectra Vista Corporation) – field portable spectroradiometer (CCNY)
- SR1900 (Spectral Evolution, Inc.) – spectroradiometer (UMB)

5.2.4. Instruments for sun photometry

These sun photometers were deployed at stations.
Microtops (Solar Light Company) – hand-held sun photometer (atmospheric aerosols and optical depth; five instruments: USM, NRL, CUNY, USF, STAR)[3].

5.3. Continuous Underway Measurements

5.3.1. Flow-through continuous measurements

The ship's sea water flow-through system was equipped with a series of bio-optical and hydrographic instruments for continuous underway sampling. The intake point at the sea chest was at a depth of 3 m. Observational data were synchronized with time and location and were monitored in real time for determining station locations across Gulf Stream fronts. The flow-through data will also be used for spatial variability analyses. The flow-through system included:

- Two ac-9s (WET Labs) – absorption, and beam attenuation/scattering spectrophotometers, one with a 0.22 μm filter, the other without, for determining total absorption, CDOM absorption, total scattering, beam attenuation, and particle absorption at nine wavelengths[2] (Stennis/USM/NRL)
- ECO BB3 (WET Labs) – backscattering at three wavelengths (469 nm, 529 nm and 652 nm; CCNY)
- FlowCam (Fluid Imaging Technologies, Inc.) – dynamic imaging particle analysis for species composition and size measurements (LDEO)
- Advanced Laser Fluorometer (ALF; WET Labs) – for determinations of CDOM and for characterizing phytoplankton functional groups based on chlorophyll and phycobilipigments
- Mini FIRe - phytoplankton photosynthetic competency, non-photochemical quenching (LDEO)
- AlgaeOnlineAnalyser (bbe Moldeanke) – for determination of Chl-*a*, and major phytoplankton groups (LDEO)
- SST (ship)
- Salinity (ship)
- Chlorophyll fluorescence voltage (ship; uncalibrated)

5.3.2. On deck continuous measurements

Several instruments were mounted onto the ship's superstructure for making continuous observations from above the water. Some of these instrument packages viewed both water and sky. During stations, some of the observations from these instruments were invalid due to the mis-orientation of the ship with respect to the sun. These details are discussed within each group's method section.

- HyperSAS (Satlantic) – above water optical system, fixed mount on ship (NASA/GSFC)
- HyperSAS-POL (Satlantic with modifications by CCNY) – above water optical system with sky polarimeter (CCNY)
- TRIoS (TRIoS GMBh) – above water hyperspectral radiometry package (JRC)[1]
- Bow-mounted HyperPro (Satlantic) – hyperspectral radiometer mounted on the bow of the ship (NASA/GSFC)

5.3.3. Other continuous measurements – from ship's onboard systems

- Acoustic Doppler Current Profiler (ADCP)
- Meteorology
    - Wind speed
    - Wind direction
    - Sea state
    - Air temperature
- Irradiance integrated from 400 nm to 700 nm (i.e."Photosynthetic Available (Ir)radiation"; PAR)

[1]Most radiometers were calibrated at the NOAA/STAR calibration facility one week prior to the cruise and one week following the cruise. See Section 6 for more on calibrations.

[2]The ac-s and ac-9 instruments were calibrated before the cruise, twice onboard during the cruise and after the cruise.

[3]The Microtops instruments were calibrated by the NASA/GSFC Aerosol Robotic Network (AERONET) prior to the cruise.

5.4. Water Sampling and Analyses

Water samples were collected at all stations and routinely from the flow-through system by four groups. At stations, the ship's CTD-rosette system was deployed for collection of ≈15 liters of water from each of 3 depths chosen to sample representative sections of the vertical structure at the given station. The three depth horizons typically included the near surface, within the mixed layer depth and near bottom in shallow water or below the subsurface chlorophyll maximum in deep water. While the ship was transiting, water samples were collected from the underway flow-through system. Depending upon the type of measurement, water samples were either stored for later analyses or processed onboard. See Section 7 for more detailed descriptions of each groups' methods. The following parameters were or will be determined from water samples:

- HPLC phytoplankton pigment analyses (NASA/GSFC)
- CDOM absorption (NASA/GSFC)
- Dissolved organic carbon (DOC; NASA/GSFC)
- Particulate organic carbon and particulate nitrogen (POC/PN; NASA/GSFC)
- Fluorometric extracted chlorophyll
  - acidification method (NOAA/STAR)
  - non-acidification narrow-band method (USF)
- Total suspended matter (TSM; NOAA/STAR)
- Particle fluorescence and digital imaging (FlowCam; LDEO)
- Variable fluorescence – Mini-FIRe (Satlantic; LDEO)
- Advanced Laser Fluorometer (ALF; LDEO)
- Phycobilipigment concentration (LDEO)
- Filter pad spectral absorption (USF)

6. Radiometer Calibration

6.1. Calibration Background

Calibration is the process relating the instrument output to the input radiometric quantity by determining sensor responsivity. In agreement with the overview presented in Zibordi and Voss [2014], comprehensive calibration of any radiometer should account for: *i*. absolute in-air responsivity to the radiometric source (either radiance or irradiance); *ii*. in-water responsivity changes due to differences between the refractive index of air and that of water; and, *iii*. correction factors to account for non-linearity, temperature dependence, sensitivity decay with time, stray light and deviation from ideal angular response. Practically, the conversion from the instrument output values to physical units of the spectral radiometric quantity $\Im(\lambda)$ (either irradiance (*E)* or radiance (*L)* at wavelength λ) should be performed using a measurement equation, e.g.,

$$\Im(\lambda) = C_{\Im}(\lambda)\, I_f(\lambda)\, \aleph(\lambda)\, \mathrm{DN}(\Im(\lambda)) \qquad (1)$$

where $C_{\Im}(\lambda)$ is the spectral in–air absolute calibration coefficient (i.e., the absolute responsivity), $I_f(\lambda)$ is the spectral immersion factor accounting for the change in responsivity of the sensor when immersed in water with respect to air, and $\aleph(\lambda)$ (for simplicity only expressed as a function of λ) corrects for any deviation from the ideal performance of the measuring system. The term $\aleph(\lambda)$ is equal to 1 for an ideal radiometer.

The term DN($\Im(\lambda)$) indicates the digital output corrected for the ambient light (i.e., the actual digital output DN($\Im(\lambda)$)* from which the dark value D0(λ), measured by obstructing the entrance optics, and the ambient light DA($\Im(\lambda)$) due to poor shielding and baffling of light sources, have been removed according to DN($\Im(\lambda)$) = [DN($\Im(\lambda)$)*−D0($\Im(\lambda)$)] − [DA($\Im(\lambda)$) − D0($\Im(\lambda)$)]. It is mentioned that for ideal measurement conditions the values of DA($\Im(\lambda)$) equals that of D0(λ).

In–air absolute radiometric calibration for irradiance sensors generally rely on a spectral irradiance source $E_0(\lambda)$ traceable to a reference standard. Common working standards in the 250–2500 nm spectral range are calibrated quartz tungsten halogen 1000 W FEL lamps [*Grum and Becherer*, 1979; *Yoon and Gibson*, 2011].

By strictly assuming *i*. point-source, *ii*. point-detector, and *iii*. narrow bandwidth centered at the wavelength λ, the absolute radiometric calibration coefficient $C_E(\lambda)$ for an irradiance sensor is determined from the output DN($E(\lambda)$) related to the input irradiance $E(\lambda)$ by applying Eq. 1 with $I_f(\lambda) = 1$. The approximate value of $E(\lambda)$ for an irradiance sensor with faceplate of the collector normal to the source is given by

$$E(\lambda) = E_0(\lambda)\frac{d_0^2}{d^2} \qquad (2)$$

where d is the distance between source and sensor, and d_0 the distance at which the value $E_0(\lambda)$ was determined.

It is stressed that the above equation is only exact for a point irradiance source and a point detector. In actuality, an extended source such as the FEL lamp cannot be considered as an ideal point source. This may require determining non-linear effects , the exact radiometric center and the sensitivity to angular alignment through experimental measurements [see discussion in *Johnson et al.*, 2014; *Zibordi and Voss*, 2014].

The in–air absolute calibration coefficient $C_L(\lambda)$ for radiance sensors is determined using a known radiance source $L(\lambda)$. This can be given by a calibrated integrating sphere or a system composed of a reflectance standard (i.e., a reflectance plaque with calibrated directional–directional reflectance) illuminated by an irradiance standard (e.g., a calibrated 1000 W FEL lamp) [*Johnson et al.*, 2014].

When considering the lamp-plaque system, $C_L(\lambda)$ is determined with Eq. 1 from the output DN($L(\lambda)$) for the related input radiance $L(\lambda)$. Assuming a radiance sensor with *i*. narrow bandwidth centered at wavelength λ and additionally *ii*. a narrow field–of–view and *iii.* the lamp positioned on axis and normal to the reflectance plaque, the radiance $L(\lambda)$ for the sensor viewing the center of the reflectance plaque at an angle θ with respect to the normal is given by

$$L(\lambda) = E(\lambda)\rho_d(\lambda,0,\theta)\pi^{-1} \qquad (3)$$

where $\rho_d(\lambda,0,\theta)$ is the bidirectional reflectance factor of the plaque for the specific viewing configuration (generally $\theta = 45$ degrees) and $E(\lambda)$ is given by Eq. 2 with distance d between lamp and reflectance plaque [*Johnson et al.*, 2014].

For the lamp/plaque method, it is essential that the radiance source fills the FOV of the radiance sensor uniformly. Because of this, in the case of appreciable deviation from the basic assumption of narrow FOV

offered by some in-water radiance sensors, the distance d needs to be chosen to satisfy both intensity and spatial and angular homogeneity requirements for the sensor under calibration.

It is finally mentioned that often the directional–hemispherical reflectance $\rho_h(\lambda,\theta)$ is provided with the reflectance plaque instead of the bidirectional reflectance factor $\rho_d(\lambda,0,\theta)$. This requires the application of a conversion factor to $\rho_h(\lambda,\theta)$. In the specific case of Labsphere (North Sutton, NH) Spectralon plaques, a convenient correction factor for the visible and near-infrared spectral region is 1.025 [*Johnson et al.*, 2014; *Zibordi and Voss*, 2014]

6.2. Calibration of Cruise Radiometers

Pre- and post-cruise calibrations of radiometers used in this cruise were conducted at the NOAA Optical Characterization Experiment Laboratory in College Park, Maryland using a NIST traceable type FEL 1000 W standard irradiance lamp #667 and an Optronic Laboratories OL-455 integrating sphere for radiance with values traceable to NIST. Before the cruise, on 4 November 2014, the NOAA/STAR HyperPro, USF HyperPro, NASA/GSFC C-OPS, UMB SBA, and the Stennis/NRL HyperTSRB radiometers were all calibrated. Directly after the cruise, on 21 November 2014, calibrations were conducted on the NOAA/STAR HyperPro, USF HyperPro, NASA/GSFC C-OPS, Stennis/NRL HyperTSRB, JRC MicroPro and the JRC TRIoS radiometers.

Figure 3 shows an example of the pre- and post-cruise calibration results for the NOAA/STAR (L_u 206) and the USF (L_u 249) radiometers. Figure 4 shows preliminary results of 1 % maximum difference in irradiance and 2 % in radiance in the 400 nm to 800 nm spectral interval in a comparison of NOAA/STAR and JRC calibration sources conducted immediately prior to the cruise.

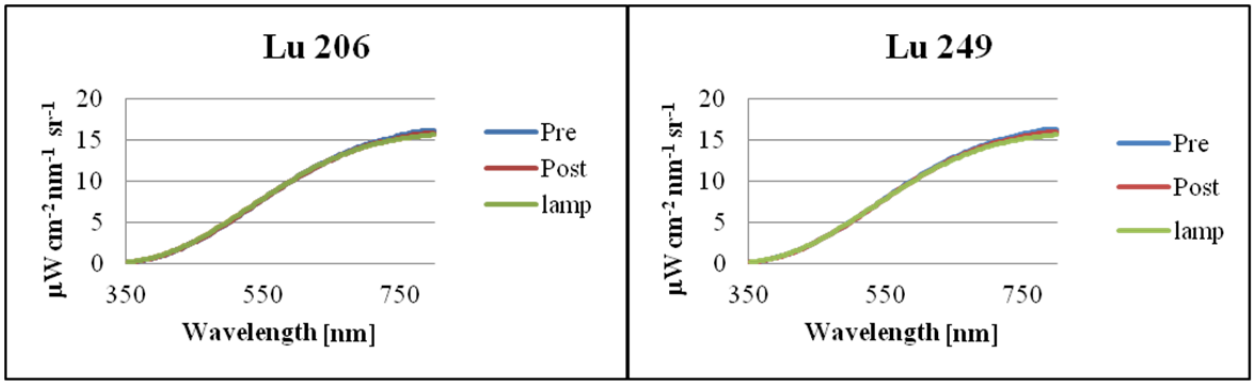

Figure 3. Example of the pre- and post-cruise calibration of the NOAA/STAR (L_u 206) and USF (L_u 249) radiance sensors used in the Nov. 2014 Cal/Val cruise. The radiances indicated as "lamp" are the values of the calibration source. The "pre–" and "post-" radiances are the measured values of the reference integrating sphere source determined using each specific instrument's original calibration.

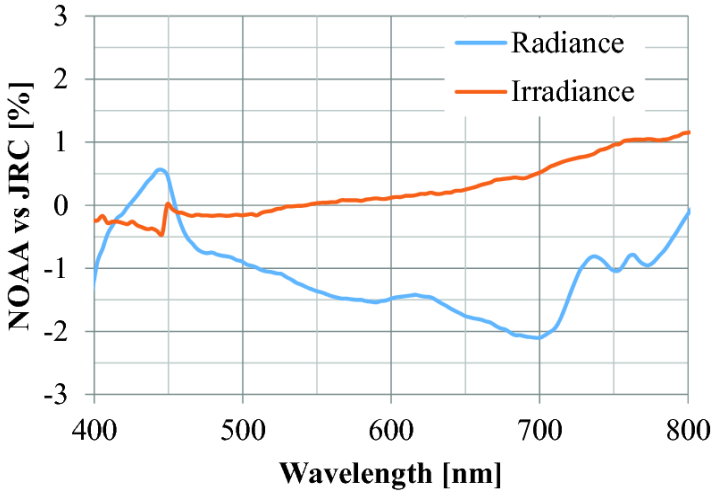

Figure 4. Spectral irradiance and radiance differences between the calibration sources applied by the JRC (i.e., the Gooch & Housego, NIST traceable type FEL 1000 W lamp #1282 for irradiance, and the same lamp illuminating a Labsphere Spectralon 99 % reflectance plaque) and the NOAA optics laboratory (i.e., the NIST traceable FEL-1000 W lamp #667 for irradiance, and an Optronics Laboratories integrating sphere OL-455) for radiance. The differences were determined using TRIoS (Rastede, Germany) irradiance and radiance spectrometers with approximately 10 nm spectral resolution.

7. Participating Science Groups' Methods and Protocols

7.1. NOAA/STAR – Michael Ondrusek and Eric Stengel

HyperPro in-water radiometry

One of the primary tools used by NOAA/STAR for in situ ocean color radiance validations is a Satlantic HyperPro Profiler II (specifications and manuals for the HyperPro can be found at http://www.satlantic.com). The HyperPro system has a downward looking HyperOCR radiometer that measures upwelling radiance ($L_u(\lambda)$) and an upward looking HyperOCI irradiance sensor to measure downwelling irradiance ($E_d(\lambda)$) in the water column. In addition there is an above-water upward looking HyperOCI irradiance sensor to measure downwelling irradiance ($E_s(\lambda)$) used as reference during data reduction. The E_s sensor was mounted on one of the poles pictured in Section 7.3 (Fig. 8). These measurements are used to calculate $nL_w(\lambda)$ spectra observed by ocean color satellites. $nL_w(\lambda)$ spectra can be used to validate satellite ocean color radiances and develop ocean color derived products such as chlorophyll *a* or TSM concentrations used in ecological studies [*Ondrusek et al.*, 2012].

The HyperPro Profiler II is deployed in a free falling mode where it is lowered and raised in the water column while taking care to keep it away from the ship and avoid ship shadowing. The weight is adjusted on the profiler to allow a descent rate of 0.1 m s^{-1} to 0.3 m s^{-1}. Each HyperOCR or HyperOCI has a 256 channel silicon photodiode array detector with a 10 nm spectral resolution and a spectral sampling of 3.3 nm $pixel^{-1}$. The instruments are calibrated from 350 nm to 900 nm. The HyperOCRs have dark signal corrections performed using shutter dark measurements collected every 5th scan. The radiometers were calibrated before and after the cruise as described in Section 6. The profiler is equipped with depth, temperature, tilt and two WET Labs ECO Puck Triplet sensors. One ECO Puck sensor measures fluorescence estimates of chlorophyll-a, CDOM and phycoerythin. The second ECO Puck sensor measures backscattering b_b at 443 nm, 550 nm, and 860 nm.

The operation of the HyperPro Profiler II instrument is described at: http://satlantic.com/sites/default/files/documents/ProfilerII-RevK-Manual.pdf. The system was deployed by hand simultaneously with the USF HyperPro Profiler II (Section 7.5), the JRC MicroPro Profiler (Section 7.3) and the NASA C-OPS Profiler (Section 7.9). For each station, the sun was positioned directly off the stern and the 4 profiling instruments were positioned evenly spaced at the stern (Fig. 5). All four instruments were lowered to the sea surface together with the ship maintaining approximately 1 knot speed to get the profilers at least 20 m off the stern. After that, the ship maintained just enough turns to prevent the profilers from closing in to the ship and to prevent them from crossing while profiling. For each station, 3 to 5 multicast measurement sets were conducted (section D of Profiler II manual). For each set, all four profilers were lowered to 10 m and raised together 3 to 5 times. If sky conditions changed significantly during the cast, the set was stopped and restarted when the conditions were favorable again. Examples of matchups between the NOAA HyperPro R_{rs} data and VIIRS ocean color satellite data are shown in Fig. 6. The NASA, CLASS and NRL data are VIIRS data processed by the NASA Ocean Color Biology Group (http://oceancolor.gsfc.nasa.gov/), NOAA's Comprehensive Large Array-data Stewardship (http://www.nsof.class.noaa.gov/) and the Naval Research Laboratory (http://www.nrl.navy.mil/), respectively.

Figure 5. Photograph of the 4 profiling radiometers that were deployed simultaneously off the stern at each station.

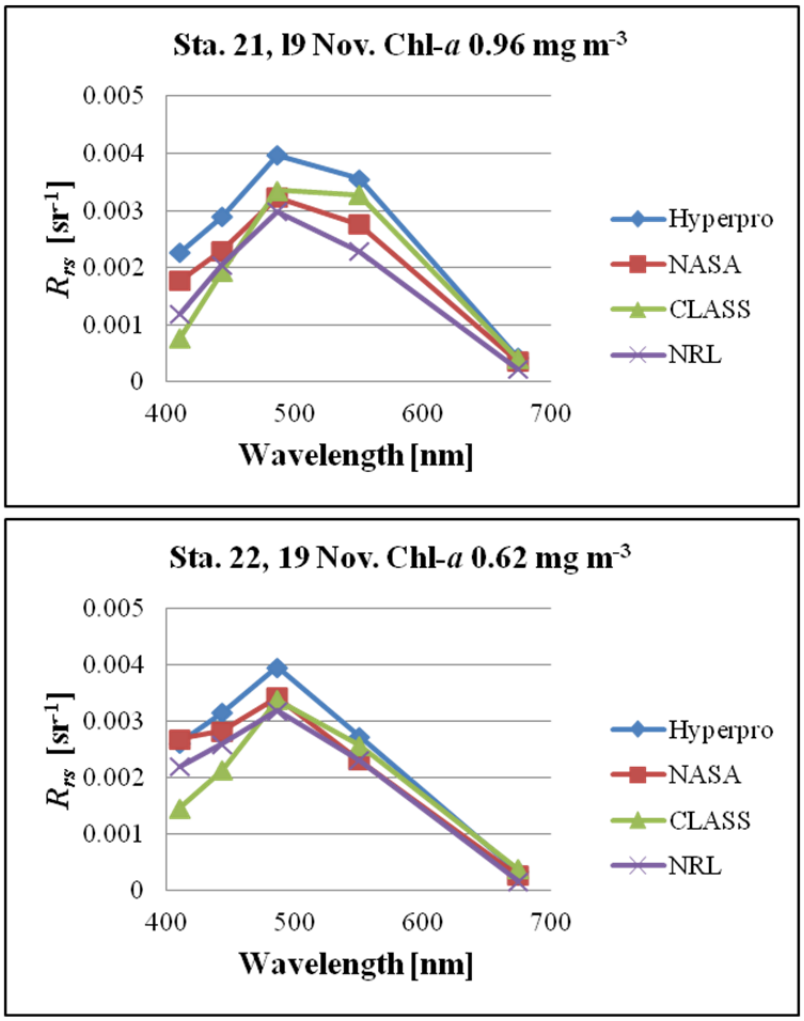

Figure 6. Preliminary VIIRS vs. NOAA HyperPro comparisons from 19 November Stations 21 and 22. VIIRS NASA and CLASS data are averages over 5x5 pixels. NRL data use a single pixel matchup.

The data were processed using Satlantic Prosoft processing software version 8.1. Normalized water-leaving radiance ($nL_w(\lambda)$) spectra are calculated using the equation:

$$nL_w(\lambda) = L_w(\lambda, 0^+) * F_0(\lambda)/E_s(\lambda) \quad (4)$$

where F_0 is the mean extraterrestrial solar irradiance [*Neckel and Labs*, 1984] and $E_s(\lambda)$ is the downwelling spectral irradiance just above the surface and is measured with the above water HyperOCR irradiance reference sensor. $L_w(\lambda)$ is the water-leaving radiance calculated just above the surface by:

$$L_w(0^+, \lambda) = L_u(0^-, \lambda) * [(1-\rho(\lambda, \theta))/n_w(\lambda)^2] \quad (5)$$

Here, $\rho(\lambda, \theta)$ is the sea surface Fresnel reflectance and is set as 0.021, and $n_w(\lambda)$ is the Fresnel refractive index of seawater and is set here as 1.345. $L_u(0^-, \lambda)$ is the calculated upwelling radiance just below the surface and is determined by using the diffuse attenuation coefficient (K_{Lu}) calculated using a least

squares regression fit from log transformed measured $L_u(\lambda)$ values and the intercept just below the surface.

ASD above-water radiometry
Above-water radiometric measurements were conducted using an ASD HandHeld2 radiometer (http://www.asdi.com/products/fieldspec-spectroradiometers/handheld-2-portable-spectroradiometer). Remote sensing reflectance, $R_{rs}(\lambda)$, measurements were conducted at seven stations and the NIST reference blue plaque comparison was conducted at two stations. Stennis/NRL protocols were followed. This includes utilizing optics which provided a 10° FOV and sampling rate of five scans each time the trigger is activated. The instrument is optimized before each set of five scans to adjust the integration time. Five scans are collected of the sky at an azimuth of 135° from the sun and 50° from the horizon with an unobstructed view of the sky. The next five scans are collected using the gray card again with an azimuth of 135° from the sun and 50° from the horizon. Finally, five scans of the water are conducted using the same scan angles using care to provide an unobstructed view.

Processing is being conducted using NRL-developed processing software that follows the guidelines of Mueller et al. [2003] and utilizes 5 different processing models including: R_{rs}_sfc (no NIR reflectance correction), R_{rs}_fresnel (Fresnel correction omitted), R_{rs}_ *Carder and Steward* [1985], R_{rs} _ *Lee et al.* [1997], and R_{rs}_ *Gould et al.* [2001].

Extracted fluorometric chlorophyll
Chlorophyll-a concentrations were measured using a Turner 10 AU Fluorometer [*Holm-Hansen et al.*, 1965]. Surface samples were collected in duplicate at each station from the CTD or flow-through system and 400 mL of seawater was filtered on a 25 mm diameter, 0.7 μm glass microfiber filter (GF/F; Whatman). The filters were extracted in 90 % acetone in a freezer for at least 48 h. The samples were vortexed then centrifuged for 5 min before being measured on the Turner 10 AU before and after acidification.

Total Suspended Matter (TSM)
TSM samples were collected in duplicate from the surface waters for each station. Up to 2 L of water were collected for each sample and processed according to techniques outlined by Hunter [2006]. Water samples were filtered on pre-weighed 47 mm diameter GF/F filters. The samples were filtered under positive pressure until the filtration stopped. The volume of the filtrate was then measured with a graduated cylinder and recorded. The filters were placed in 47 mm diameter Petri dishes and oven dried at 60 °C for 12 h then stored in a desiccator until analysis. The filters were weighed on a Sartorius CPA 2250 balance (with a precision of 0.01 μg) and weighed at least three times until consecutive readings were less than 0.055 % variable [*EPA*, 1971].

7.2. U. Miami– Kenneth J. Voss

NURADS measurements of the BRDF or Radiance Distribution
This instrument measures the spectral upwelling radiance distribution [*Voss and Chapin*, 2005]. The upwelling light field from the same water type in the ocean varies with the illumination geometry and the viewing geometry. Almost all measurements of the upwelling radiance used for satellite validation/calibration are made in the nadir direction (instrument looking straight down, light coming straight up), however the satellite views the ocean at a different angles, depending on where the specific pixel is in the satellite scan line. To relate the measurement made on the ground to what the satellite is viewing requires information on the variation of the radiance with direction, which is the radiance distribution. The shape of the radiance distribution also changes spectrally, so the spectral variation of the radiance distribution must also be determined. This is exactly the parameter that NURADS measures. The model that is used to correct for the oceanic BRDF in the data reduction process of satellite data is provided in Morel et al. [2002]. This model has been validated several times [*Gleason et al.*, 2012; *Voss*

and Morel, 2005; *Voss et al.*, 2007], but the model is aimed at Case I waters (water parameters determined by a statistical relationship with chlorophyll *a*), and breaks down in coastal waters. While we have taken a considerable amount of open ocean radiance distribution data, and some coastal radiance distribution data, because of the variability of the water properties in the coastal area it is reasonable to expand the data set and to take radiance distribution data along with other validation data when doing experiments such as this.

The NURADS instrument was calibrated following previously published protocols [*Voss and Zibordi*, 1989; *Voss and Chapin*, 2005]. Mike Ondrusek (NOAA/STAR) deployed the instrument at stations in conjunction with other instruments as described elsewhere (Sections 5.2, 7.1 and Table A-2). Floats were attached to the instrument to allow it to measure at the surface, 20 m to 50 m away from the ship (measurement depth is 0.75 m). When deployed, the instrument measures the upwelling radiance continuously, cycling through the 6 different wavelengths and associated dark measurements. NURADS measurements were made at 5 stations (11, 17, 21, 22 and 23).
The data are currently being reduced and quality controlled.

7.3. JRC – Giuseppe Zibordi and Marco Talone

MicroPro

In–water free-fall radiometry (i.e., radiometers operated on free-fall systems) is conveniently applied to produce continuous profiles of upwelling radiance $L_u(z,\lambda,t)$, downward irradiance $E_d(z,\lambda,t)$ and also upward irradiance $E_u(z,\lambda,t)$ at depths z, wavelength λ and time t. Additionally, the above–water downward irradiance $E_d(0^+,\lambda,t)$ (indicated as $E_s(\lambda)$ in section 7.1) is measured to minimize the effects of illumination changes on in–water radiometric measurements during data collection. The in–water profile data are used to extrapolate to 0^- (i.e., just below the water surface) the radiometric quantities which cannot be directly measured because of wave perturbations. The accuracy of sub-surface radiometric products largely depends on the sampling depth-interval and on the depth resolution [*D'Alimonte et al.*, 2010; *Zaneveld et al.*, 2001]. In general highly accurate in–water radiometric products can only be determined by sampling near the surface (especially in coastal regions due to possible vertical non-homogeneities in the optical properties of seawater) and, by producing a large number of measurements per unit depth not significantly affected by tilt to minimize perturbations due to wave effects [*Zibordi et al.*, 2004].

In agreement with common practice [e.g., see *Zibordi and Voss*, 2014], reduction of free-fall radiometric data $\Im(z, \lambda, t)$ (i.e., $L_u(z,\lambda,t)$, $E_u(z,\lambda,t)$ and $E_d(z,\lambda,t)$) requires minimization of perturbations created by illumination change during data collection. This is performed according to

$$\Im_0(z,\lambda,t_0) = \frac{\Im(z,\lambda,t)}{E_d(0^+,\lambda,t)} E_d(0^+,\lambda,t_0) \qquad (6)$$

where $\Im_0(z, \lambda, t_0)$ indicates radiometric values as if they were all taken at the same time t_0, and $E_d(0^+,\lambda,t_0)$ specifies the above–water downward irradiance at time t_0 (with t_0 generally chosen to coincide with the beginning of the acquisition sequence). The sub-surface quantities $\Im_0(0^-, \lambda, t_0)$ (i.e., $L_u(0^-,\lambda,t_0)$, $E_u(0^-,\lambda,t_0)$ and $E_d(0^-,\lambda,t_0)$) are then determined as the exponentials of the intercepts resulting from the least-squares linear regressions of $\ln \Im_0(z, \lambda, t_0)$ versus z within the extrapolation interval identified by $z_1 < z < z_2$ and chosen to satisfy the requirement of linear decay of $\ln \Im_0(z, \lambda, t_0)$ with depth. The negative values of the slopes of the regression fits are the so-called diffuse attenuation coefficients $K_\Im(z_1, z_2, \lambda, t_0)$ (i.e., $K_l(z_1, z_2, \lambda, t_0)$, $K_u(z_1, z_2, \lambda, t_0)$ and $K_d(z_1, z_2, \lambda, t_0)$) determined from $L_u(z,\lambda,t)$, $E_u(z,\lambda,t)$ and $E_d(z,\lambda,t)$ values, respectively, from the selected extrapolation interval.

Omitting the variable t, the radiometric quantity of major relevance is the so-called water–leaving radiance $L_w(\lambda)$. This is the radiance leaving the sea quantified just above the surface from

$$L_w(\lambda) = 0.543\, L_u(0^-, \lambda) \qquad (7)$$

where the factor 0.543 is assumed independent of wavelength [*Austin*, 1974] and accounts for the reduction in radiance from below to above the water surface.

The radiometric quantity of major relevance for satellite ocean color investigations is the remote sensing reflectance $R_{rs}(\lambda)$ given by

$$R_{rs}(\lambda) = \frac{L_w(\lambda)}{E_d(0^+, \lambda)}. \qquad (8)$$

It must be noted that $R_{rs}(\lambda)$ is thus corrected for illumination conditions depending on sun zenith angle, sun-earth distance and atmospheric transmittance [*Mueller et al.*, 2003].

The JRC MicroPro free-fall radiometer system produced by Satlantic L.P. (Halifax, Canada), is equipped with OCR-507 radiometers for $L_u(z,\lambda,t)$, $E_u(z,\lambda,t)$, $E_d(z,\lambda,t)$ and $E_d(0^+,\lambda,t)$ measurements (Fig. 7). These sensors provide data at 6 Hz in seven spectral bands with 10 nm bandwidth centered at nominal wavelengths of 412 nm, 443 nm, 490 nm, 510 nm, 555 nm, 665 nm and 683 nm. The L_u sensor has approximately 18° in-water full-angle field of view (FAFOV). Each MicroPro measurement sequence includes data from multiple casts (i.e., multicasting [*Zibordi et al.*, 2004]) performed with a deployment speed of approximately 0.3 ms^{-1}.

During the 2014 VIIRS Cal/Val Cruise, measurements were performed during each station. At the end of each station, diffuse to direct irradiance measurements were performed by operating a shadow-band in conjunction with the above-water E_d sensor (Fig. 8). Out of the 23 measurement stations carried out during the cruise, 8 were performed under ideal illumination conditions (i.e., low cloud cover and sun clear from clouds).

Figure 7. MicroPro free-fall with E_d and L_u sensors located on the lateral side of the fins and an E_u sensor located on the lowest side of the system hub.

Figure 8. Poles utilized to deploy the various above-water E_d reference sensors. The shadow-band was operated in conjunction with the MicroPro above-water E_d reference sensor to determine the diffuse to direct irradiance ratio required to compute self-shading correction factors for in-water L_u and E_u data.

MicroPro data products were determined in agreement with common practice [*Zibordi and Voss*, 2014] by applying equations 6-8, choosing an extrapolation interval of 0.3 m to 3.0 m and applying corrections for the non-cosine response of the above-water E_d reference sensor [*Zibordi and Bulgarelli*, 2007] and self-shading of L_u and E_u sensors [*Gordon and Ding*, 1992; *Mueller et al.*, 2003; *Zibordi and Ferrari*, 1995] where the required seawater absorption a is approximated through the diffuse attenuation coefficient K_d.

An analysis of the uncertainties affecting the normalized water-leaving radiance $nL_w(\lambda)$ determined from MicroPro, on a first approximation assumed representative for $R_{rs}(\lambda)$, indicated values in the range of approximately 4 % to 5 % in the selected spectral region for moderately sediment dominated waters [see *Zibordi and Voss*, 2014]. The uncertainty sources considered were: *i.* uncertainty of the absolute in–air radiance calibration [*Hooker et al.*, 2002] and immersion factor [*Zibordi*, 2006] for the L_u sensor (i.e., 2.7 % and 0.5 %, respectively, composed statistically); *ii.* uncertainty of the correction factors applied for removing self-shading perturbations computed as 25 % of the applied corrections; *iii.* uncertainty of the in-air irradiance calibration of the above-water E_d sensor [*Hooker et al.*, 2002] and uncertainties of the correction applied for the non-cosine response of the related irradiance collectors [*Zibordi and Bulgarelli*, 2007] (i.e., 2.3 % and 1 % respectively, composed statistically); *iv.* uncertainty in the extrapolation of sub-surface values due to wave perturbations and, changes in illumination and seawater optical properties during profiling, cumulatively quantified as the average of the variation coefficient of $nL_w(\lambda)$ from replicate measurements. In the evaluation of the proposed uncertainty values, it is mentioned that they rely on the assumption of fully independent calibrations of E_d and L_u sensors (i.e., as obtained with different lamps and laboratory set-ups). Thus, the use of the same calibration lamp and set-up (commonly applied for MicroPro radiometers) leads to a reduction of approximately 1 % of the previously declared quadrature sum of spectral uncertainties for $R_{rs}(\lambda)$ [*Gergely and Zibordi*, 2014].

.

The quality of JRC MicroPro radiometric products (Fig. 9) has been evaluated through quality-indices determined during the data processing. These include: *i.* changes in illumination conditions during profiles are quantified through the standard deviation of $E_d(0^+,\lambda, t)$ at each λ; *ii.* difficulties in the determination of subsurface extrapolated quantities determined by a small number of measurements per unit depth, significant differences between $E_u(z, \lambda, t_0)/L_u(z, \lambda, t_0)$ at different depths in the extrapolation interval, or large differences between $E_d(0^-, \lambda, t_0)$ and $E_d(0^+, \lambda, t_0)$; *iii.* poor illumination conditions, resulting from high sun zenith angles or cloudiness, both quantified through values of the diffuse to direct irradiance ratio $r(\lambda)$ exceeding thresholds.

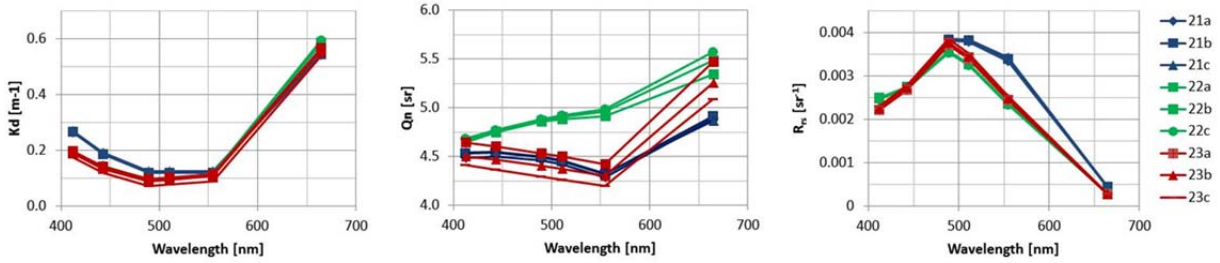

Figure 9. Sample $R_{rs}(\lambda)$ data from the MicroPro system. Data refer to measurement stations 21 (blue), 22 (green) and 23 (red). The left panel illustrates $K_d(\lambda)$ values, the central panel shows Q_n (i.e., E_u/L_u) and the right panel is $R_{rs}(\lambda)$.

TRIoS

The JRC TRIoS (Rastede, Germany) above-water optical system is composed of two pairs of RAMSES ARC-VIS hyperspectral radiometers measuring $L_T(\theta, \Delta\phi, \lambda)$ and $L_i(\theta', \Delta\phi, \lambda)$ and two RAMSES ACC-VIS for $E_d(0^+,\lambda)$ (Fig. 10). Measurements are performed in the 400 nm to 900 nm spectral range with resolution of approximately 10 nm for the output data. The nominal FAFOV of radiance sensors is 7° for one unit and 3° for the second. The rationale for different FOVs is the interest in evaluating the effects of glint perturbations with different sensor footprints at the surface and different integration times.

The measurement method relies on L_T and L_i sensors simultaneously operated on the same mounting frame with identical azimuth plane and with $\theta = 40°$ and $\theta' = 140°$, respectively. Measurement sequences are performed with user-definable intervals and frequencies, and integration time varying automatically depending on the brightness of the target. The deployment frame is manually adjusted for each measurement sequence to satisfy the requirement of $\Delta\phi$ (the relative azimuth angle between the sun and the instrument viewing direction) is 90°. Care is put in looking at the surface at a distance from the ship minimizing superstructure perturbations in measurements [*Hooker and Zibordi*, 2005].

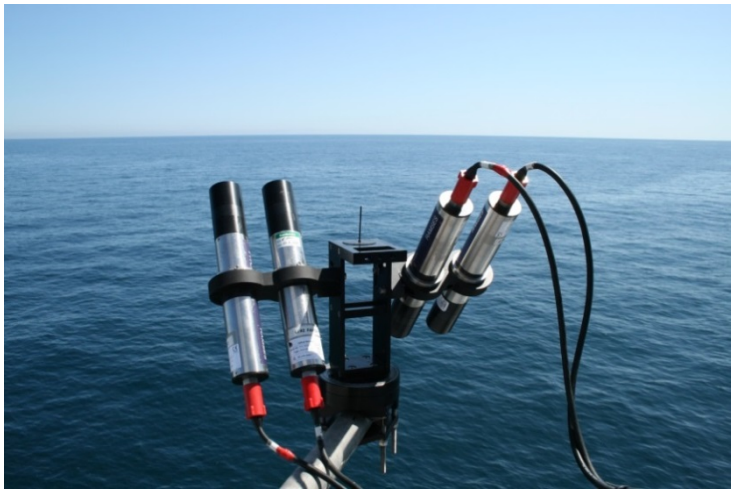

Figure 10. TRIoS radiometer system operated on its mounting frame. One unit (i.e., one L_T and one L_i sensors) has factory-standard 7° FOV. The other unit has custom 3° FOV. The related above-water E_d sensors have been operated in conjunction with all other above-water E_d radiometers.

Values of $R_{rs}(\lambda)$ are determined in agreement with common practice [*Zibordi and Voss*, 2014]. The minimization of the effects of glint perturbations in $L_T(\theta, \Delta\phi, \lambda)$ and possibly the effects of cloud perturbations in $L_i(\theta', \Delta\phi, \lambda)$ is achieved by deriving the related values from the average of independent measurements satisfying strict filtering criteria [*Zibordi*, 2012; *Zibordi et al.*, 2009].

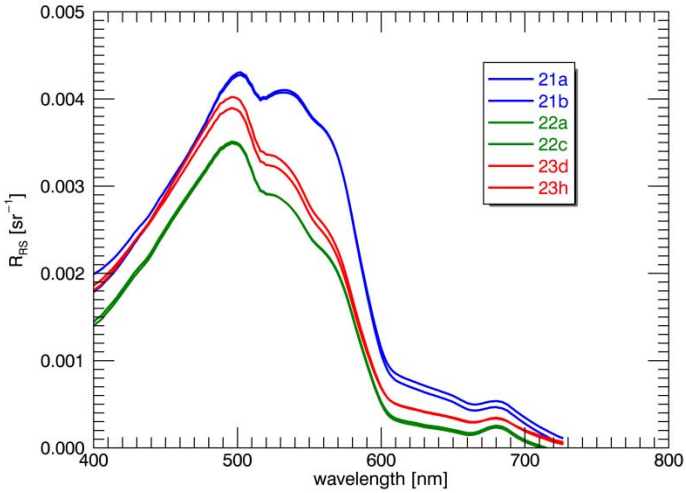

Figure 11. Sample $R_{rs}(\lambda)$ data from the TRIoS 7° FOV system. Data refer to measurement stations 21 (blue), 22 (green) and 23 (red).

Estimated uncertainties of TRIoS $R_{rs}(\lambda)$ data from previous investigations performed in moderately sediment dominated waters [*Zibordi et al.*, 2012] indicate values of approximately 4 % to 6 % in the blue-red spectral regions. These were determined accounting for contributions from: *i.* uncertainty of the absolute radiance calibration for L_T and L_i sensors; *ii.* uncertainty of corrections for the off-nadir viewing geometry computed as 25 % of the applied correction factors (these relatively large percent values are expected to account for uncertainties due to the intrinsic assumption of Case 1 water); *iii.* straylight and

polarization effects; *iv.* non-cosine response of the irradiance sensor; *v.* environmental perturbations (e.g., wave effects, changes in illumination and seawater optical properties during measurements) quantified as the average of the variation coefficient obtained from $R_{rs}(\lambda)$ values from replicate measurements.

The quality control of $R_{rs}(\lambda)$ measurements mostly includes checking for high variance of multiple sea- and sky-radiance measurements [see *Zibordi et al.*, 2009]. During the oceanographic cruise, TRIoS measurements (see Fig. 11) were performed at 12 measurement stations. Out of these, data at 5 stations are considered to fully satisfy the most strict quality criteria.

7.4. UMB – Zhongping Lee, Jianwei Wei and Junfang Lin

In situ Measurements of the Water Color and IOPs in Northwest Atlantic Ocean

1. Specific Objectives:

- In situ measurement of the remote sensing reflectance $R_{rs}(\lambda)$ by directly measuring the water-leaving radiance, $L_w(\lambda)$. The data will be used for inter-comparison with data collected from other instruments/platforms and validation of the VIIRS ocean color products.
- In situ measurement of the IOPs including a_t, c_t, and b_b, a_g, c_g, to evaluate the measurement uncertainty of such instruments and to validate the VIIRS ocean color products.

2. Instruments and Methods

SBA system

To characterize the water optical properties, we measured the remote sensing reflectance $R_{rs}(\lambda)$ using the SBA scheme [*Lee et al.*, 2013]. Based on the Satlantic's hyperspectral radiometric profiler, the SBA system is equipped with one hyperspectral irradiance sensor (HyperOCI, Satlantic Inc) measuring the above-water downwelling plane irradiance (E_s) and one hyperspectral radiance sensor (HyperOCR, Satlantic Inc) which simultaneously records the water-leaving radiance $L_w(0^+, \lambda)$ by blocking off the surface-reflected skylight with a cone (Fig. 12).

The Satlantic's hyperspectral radiometers are fully digital optical packages. HyperOCR has an FOV of 11.4° in air (8.5° in water).

The radiance can be measured at about 3 nm increments from ultraviolet (≈350 nm) to near-infrared (≈800 nm) wavelengths with a wavelength accuracy of ±0.1 nm. And each spectral band is approximately 10 nm wide. HyperOCI is a cosine response collector, with an accuracy within ±3 % over 0° to 60° and ±10 % over 60° to 85°.

Both radiometers were calibrated by the manufacturer and further validated at NOAA/STAR Optical Characterization Experiment Laboratory. During deployment, the instrument package was always kept >20 m away from the ship to avoid shadows or reflections of the ship hull. For the measured E_s and $L_w(0^+, \lambda)$ data pairs, only those with inclination less than 5° were used for further analysis. The E_s was interpolated spectrally so as to match the wavelengths of the L_w sensor. The instantaneous remote sensing reflectance was first determined as the ratio of instantaneous $L_w(0^+, \lambda)$ to the corresponding E_s as in Eq. 8 above. The derived reflectance time series, $R_{rs}(\lambda, t)$, was then subjected to a threshold filtering. The filtering procedure is critical for quality assurance of R_{rs} data, because some of the $R_{rs}(\lambda, t)$ data were contaminated when the cone popped out of the water surface and the L_w sensor received the light reflected off the sea surface, or when the L_w sensor window was immersed into the water. To start, the first

mode of the $R_{rs}(698, t)$ data sequence was located from its probability density function. Then, all those measurements of $R_{rs}(\lambda, t)$ with $R_{rs}(698, t)$ beyond ±15 % of the model were filtered out. The remaining $R_{rs}(\lambda, t)$ spectra were used to derive the median $R_{rs}(\lambda)$ spectrum at each station.

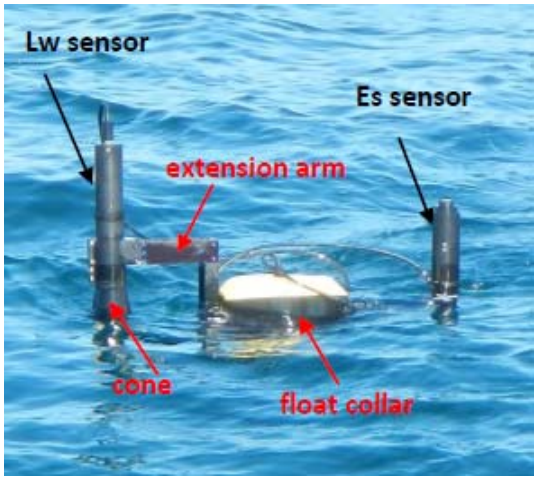

Figure 12. Measuring R_{rs} using the skylight-blocked approach (SBA). As shown in the figure, the radiometer on the left side of fin looks downwards and directly measures the water-leaving radiance L_w, while the radiometer on the right simultaneously observe the above-water downwelling plane irradiance E_s.

IOP instrument package

Two ac-s spectrophotometers (WET Labs) were integrated with one backscattering meter (BB7FL2, WET Labs) to measure IOPs. The ac-s meter measures the absorption, a, and attenuation, c, coefficients at more than 80 wavelengths between 400 nm to 732 nm. One ac-s was used to measure the total a and c,

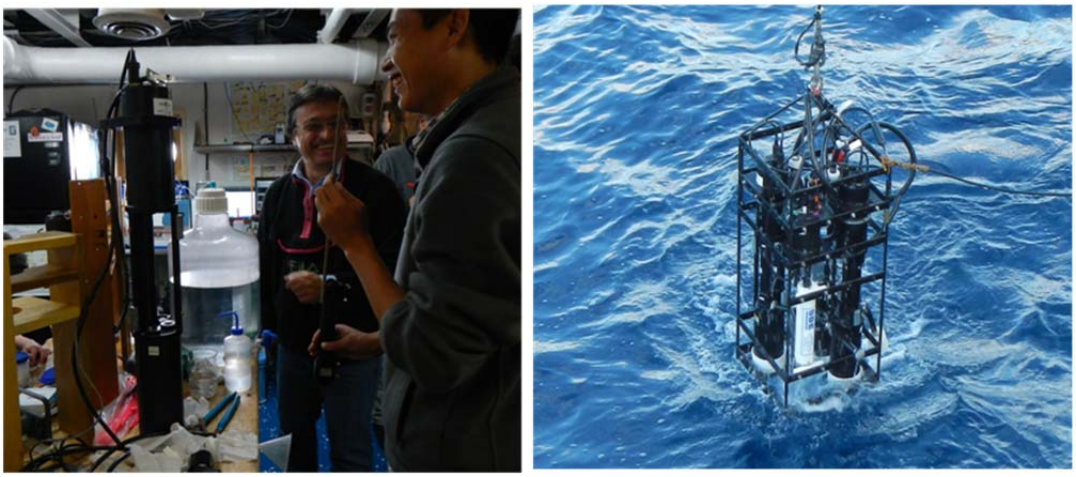

Figure 13. Pure water calibration of ac-s meter onboard (left panel) and deployment of instrument package (right panel).

while another one was equipped with a Whatman PolyCap TF filter (0.2 μm nominal diameter) to measure the CDOM absorption a_g and CDOM attenuation c_g. BB7FL2 meter measures the backscattering coefficient at seven wavelengths (412 nm, 440 nm, 488 nm, 532 nm, 595 nm, 695 nm and 715 nm) and the CDOM and chlorophyll fluorescence at two wavelengths.

All instruments were calibrated by their manufacturer. In the field, the ac-s spectrophotometers were also monitored with ultra-pure water (Milli-Q), according to the recommended procedure [*Sullivan et al.*, 2006]. The IOP package was deployed to profile the water column from surface down to 40 m (Fig. 13). All the raw data, including CTD data, were logged simultaneously.

Spectral Evolution Radiometer

The SR-1900 spectraoradiometer (Spectral Evolution, Inc) measured the sky radiance (L_{sky}) and the total of surface-reflected sky radiance and water-leaving radiance (L_{ref}+L_w), and the downwelling plane irradiance (E_s). The measurements were recorded at 768 wavelengths from 350 nm to 1900 nm. The spectral resolution is 4 nm from 350 nm up to1000 nm and 10 nm from 1000 nm up to 1900 nm. When measuring L_{sky} and L_{ref}+L_w, the radiometer was pointed to the target at 90° azimuth direction relative to the sun and 30° zenith angle.

3. Database Summary

We collected R_{rs} data at 18 stations and IOP data at 20 stations throughout the cruise. Most of the measurements were completed under cloudy skies. At 16 stations, both R_{rs} and IOPs were measured simultaneously (<2 h apart). The SR-1900 data were obtained at 11 stations. The time difference between SBA and SR-1900 measurements were less than one hour.

4. Preliminary Results/Examples

We have processed all the R_{rs} measurements. These data were corrected for self-shading effect following the relationship of *Gordon and Ding* [1992]. Sample data in the blue oceanic waters are presented in Fig. 14. These data were collected on 13 November 2014 with solar zenith angle between 50° to 70° and surface waves between 1 m to1.5 m high. The SBA-measured remote sensing reflectance spectra have very high repeatability. The low remote sensing reflectance at blue-UV bands suggests that the water constituents in this region are likely dominated by CDOM absorption.

The IOP measurements and Spectral Evolution data are currently under processing.

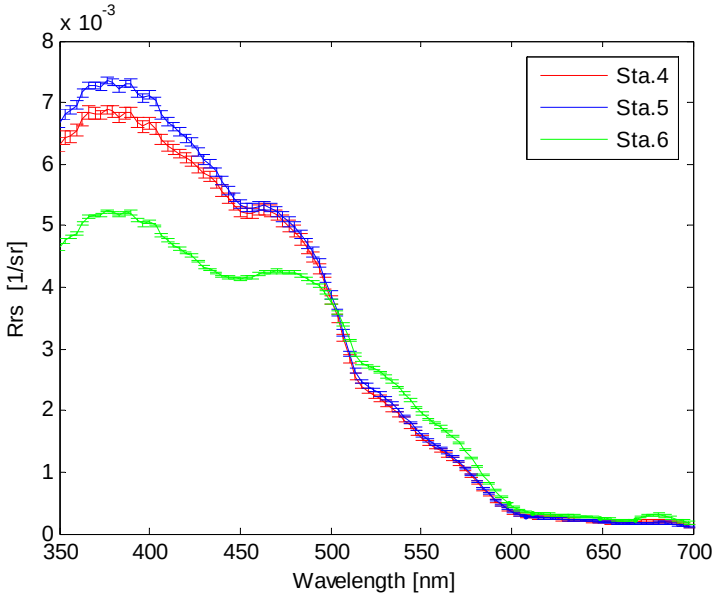

Figure 14. Remote sensing reflectance $R_{rs}(\lambda)$ measured by SBA instrument. The error bars denote the standard deviation of the $R_{rs}(\lambda)$ measurements.

7.5. USF – Chuanmin Hu, David English, Charles Kovach and Jennifer Cannizzaro

Spectral absorption and pigment determinations

Understanding the variability in chlorophyll-specific phytoplankton absorption spectra, $a^*_{ph}(\lambda)$, is essential for primary production modeling, calculation of underwater light field characteristics, and development of remote sensing algorithms for estimating Chl-*a* concentrations. The spectral absorption of particles suspended in the water can be assessed by filtering a water sample through a glass fiber filter and quantifying the spectral transmission of the filter relative to a wetted blank. The subsequent methanol extraction of the pigments from the particles captured by the filter followed by re-measurement of both filters allows for the total particulate absorption to be separated into living (or pigmented) and non-living (or detrital) components [*Kishino et al.*, 1985]. The extraction of pigments from the particles also enables Chl-*a* to be determined fluorometrically [*Holm-Hansen and Riemann*, 1978; *Welschmeyer*, 1994].

At each station, Niskin bottles were used to collect water samples from just below the water surface and from a second depth lower in the photic zone. The samples were used for assessment of the chlorophyll *a* concentration, as well as the particulate, $a_p(\lambda)$, and detrital, $a_d(\lambda)$, absorption spectra. Duplicate samples were collected at selected stations. Aliquots were filtered using low vacuum pressure (<10 cm Hg) to concentrate the particles for pigment and absorption determination onto a glass fiber GF/F (Whatman) filter. These filters were placed into containers and quickly frozen using liquid nitrogen. Samples were kept frozen, stored at -80˚C until analysis.

Chl-*a* and a_p data were computed for the 47 water samples collected during the cruise. The surface waters of Station 2 had the least Chl-*a* (0.18 mg m^{-3}), while surface waters of station 17 contained the greatest concentration of Chl-*a* (5.4 mg m^{-3}). Example a_p and a_d spectra are shown in Fig. 15.

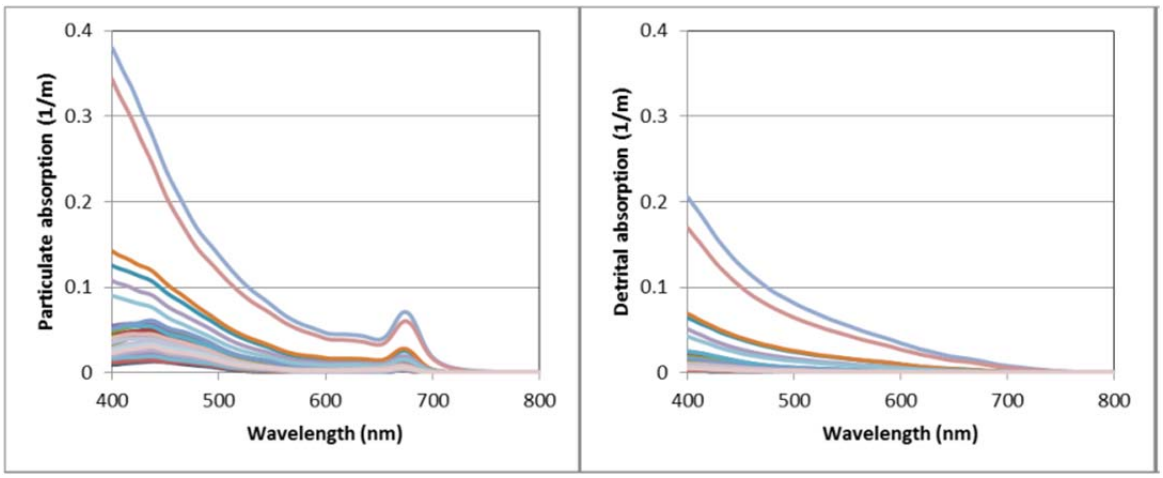

Figure 15. Particulate and detrital absorption spectra derived from water samples.

Shipboard remote sensing reflectance

Spectral observations of surface waters have led to a better understanding of not only the absorption and transmission of light below that surface, but also of phytoplankton ecology and algal bloom dynamics. By analyzing the remote sensing reflectance, researchers can infer information about the material in the near surface waters and improve algorithms for the analysis of airborne and satellite imagery. In situ measurements aid the interpretation and field validation of satellite imagery and can be used to assess plankton blooms, monitor sediment discharge, and develop climate models.

Above water $R_{rs}(\lambda)$ estimates were made using a ASD Inc. HandHeld2-Pro spectroradiometer. This instrument measures radiance at <3 nm spectral resolution for wavelengths from ≈350 nm to >1000 nm. Multiple spectra were collected for each $R_{rs}(\lambda)$ measurement.

Measurements were made of the radiance reflected from the sky, water surface, and a gray reference plaque [*Carder and Steward*, 1985; *Mueller et al.*, 2003]. Sea surface measurements were made while viewing the water with a ≈30° zenith angle and at an azimuth angle of 90° to 120° relative to the sun. Sky measurements were made at a complementary zenith angle for the sea surface measurement, at the same azimuth orientation. The HandHeld2-Pro was held >30 cm above a level reference plaque during the gray card measurement. The instrument's field of view was constrained to ≈7.5°, and its integration time was kept constant throughout the series of gray, water, and sky measurements. Additional measurements of the NIST blue reflectance plaque were made at several stations.

$R_{rs}(\lambda)$ measurements were made at 10 stations, and satisfactory $R_{rs}(\lambda)$ estimates were derived for 8 of the stations. Measurements made at Stations 2, 3, 5, 10, 11, 13, and 17 were collected using the USF Optical Oceanography Lab R_{rs} protocol. Additional measurements using USF's HandHeld 2 spectroradiometer were made by NRL at Stations 20, 21, and 23 using NRL protocols. The integration time was incorrectly recorded at stations 21and 23, requiring the use of an assumed integration time for the estimation of $R_{rs}(\lambda)$ at these 2 stations. The median $R_{rs}(\lambda)$ estimates from an open ocean and coastal station (2 and 17, respectively) can be compared in Fig. 16.

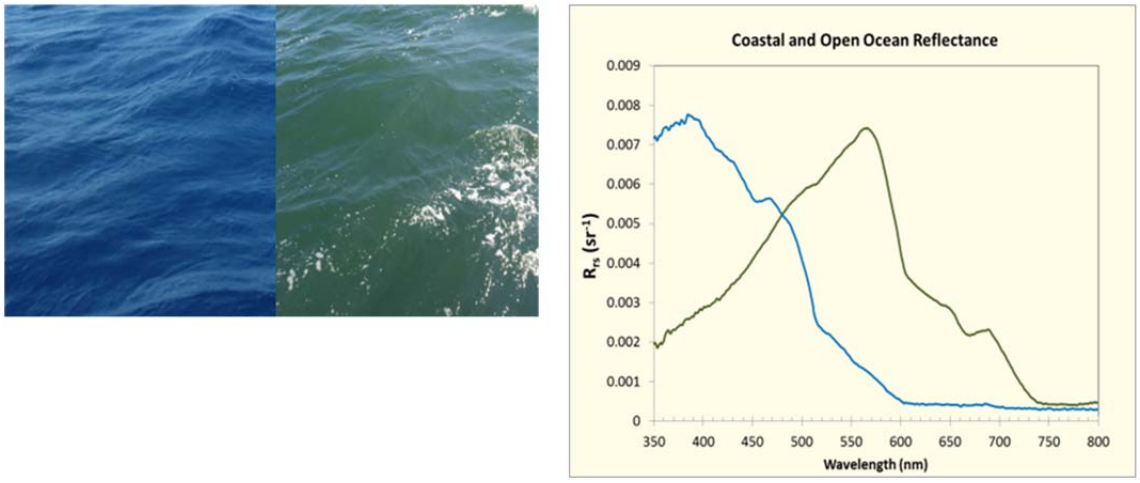

Figure 16. Pictures of the sea surface at stations V_02 (open ocean) and V_17 (coastal), and median remote sensing reflectance estimates for those stations (blue & green lines, respectively).

Near-surface light field profiling

As an appropriately oriented pair of spectrometers falls through a water column, it can measure the changes in ambient light spectra. Vertical profiles of upwelling radiance and downwelling irradiance allow computation of the in situ remote sensing reflectance as well as a spectral assessment of the available light within the water column. Extrapolation of the measurements made at multiple depths to the ocean surface allows estimation of the remote sensing reflectance of the sea surface, and can provide validation data for ocean color satellites. Examples of the information that are produced from light field profiles include estimates of light attenuation, remote sensing reflectance, energy fluxes and light available for photosynthesis.

Vertical profiles of the light available in the euphotic zone were collected using a Satlantic HyperPro-II. The Satlantic HyperPro-II is an integrated spectrometer system designed to measure ocean color as it

descends through the euphotic zone. It concurrently measures depth, temperature, conductivity, backscattering of red light, and fluorescence from chlorophyll and dissolved material. The unit is equipped with two hyperspectral radiometers, one facing upward and the other downward. The sensors incorporated into this instrument system include pressure, temperature, conductivity, and tilt sensors, in addition to a WETLabs ECO Puck Triplet and an above-water hyperspectral radiometer.

Data from the Satlantic HyperPro-II is available for most of the stations of this cruise (exceptions: Station 13, and partial data loss at Station 18) and has been converted into scientific units. The data from the HyperPro-II was initially processed using Satlantic's Prosoft 8.1 software. It was deployed using the manufacturer's recommended protocol [*Satlantic*, 2003; 2004] under the supervision of personnel from the Center for Satellite Applications and Research of NOAA's Satellite and Information Service.

Sun photometer measurements

The direct solar irradiance was measured at several stations using a Microtops II sunphotometer from Solar Light Co. Measurements from this hand-held instrument can be used to estimate atmospheric optical thickness for the sampling area. This estimate of the atmospheric absorption of light is used to support the atmospheric correction process.

Though this particular instrument was intended to serve as backup instrumentation for other groups, measurements were made at Stations 2, 10, 11, 17 & 18 using the manufacturer's recommended protocol [*Solar_Light_Company_Inc*, 2003]. The data from these shipboard measurements has not yet been analyzed.

7.6. CCNY – Alex Gilerson, Sam Ahmed, Amir Ibrahim, Ahmed El-Habashi and Robert Foster

Three instruments were used by CCNY group for above water observations: GER, SpectraVista, NY, ASD HandHeld2, ASD, CO and HyperSAS-POL, Satlantic, Canada, modified by CCNY (Fig. 17). Additionally, an ECO BB3 was included in the flow-through instrument system.

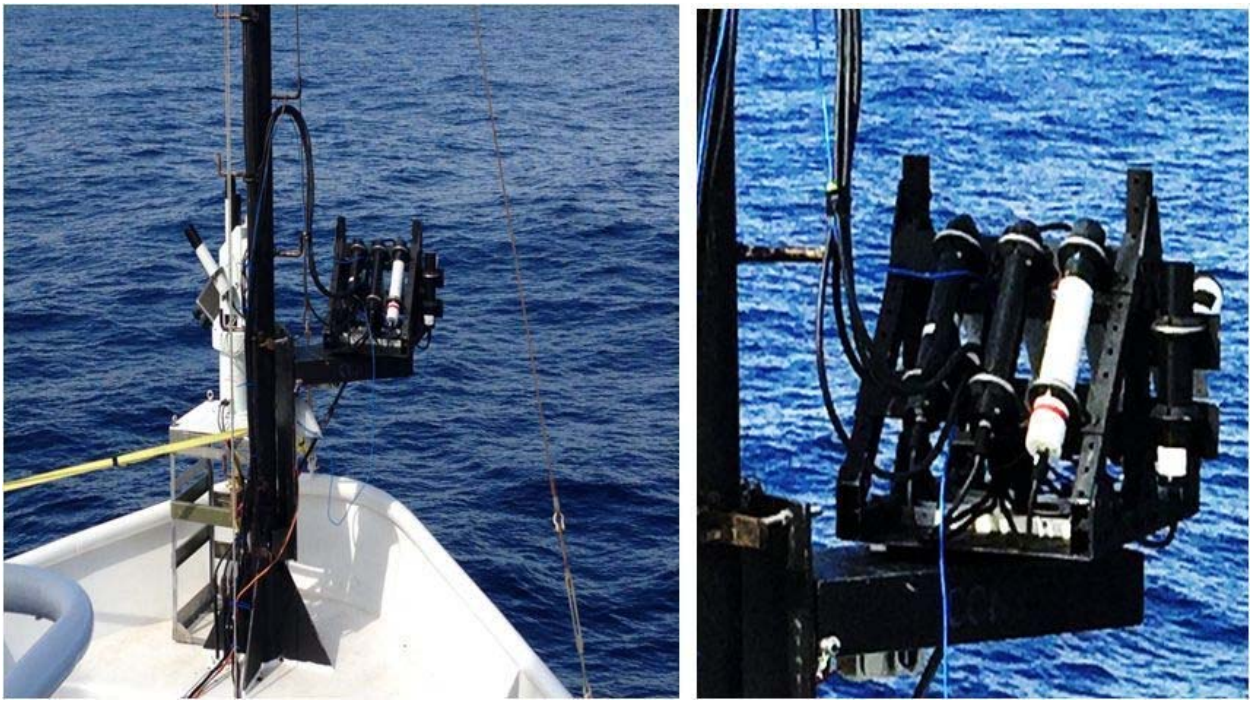

Figure 17. HyperSAS-POL on the mast at the bow of the ship.

The GER 1500, Field Portable Spectroradiometer is a hand-held spectroradiometer designed to provide fast spectral measurements covering the UV, Visible and NIR wavelengths from 350 nm to 1050 nm at 3 nm full width half maximum (FWHM) resolution. It uses a diffraction grating with a silicon diode array that has 512 discrete detectors and reports results at 512 spectral bands. A total of 482 spectral readings can be stored within its memory. Subsequent download and analysis is done using a personal computer with a standard RS232 serial port and the GER 1500 licensed operating software. The GER 1500 is equipped and operated with a lens with 4° nominal FOV for above water observations. The GER 1500 is used in the field to calculate remote sensing reflectance (R_{rs}) by measuring the total radiance (L_t) above the sea surface, the sky radiance (L_{sky}) and the downwelling radiance (L_d). The instrument has undergone radiometric and wavelength calibration in the optics mode (with the lens) at the manufacturer before the cruise but due to the nature of the measurement, calibration is not necessary.

In order to acquire L_t the instrument was placed at the azimuth angle ≈90° from the sun and 40° viewing angle from the nadir and four consecutive measurements were made. The sky radiance was measured by pointing the instrument at the sky at the same azimuth angle and 40° viewing angle from the zenith, making four consecutive measurements. L_d data were obtained by pointing the instrument at the Spectralon reference plaque; also four consecutive measurements were made. Typically, a white reference plate was used with reflectance coefficient. In addition, at some stations a gray plaque (from other groups) was used and the NIST blue tile comparison was conducted at several stations. All measurements were executed in TAR (target) mode. Downwelling irradiance is determined as $E_d = A*\pi *L_d$, where $A = 0.99$ is the reflectance factor of the white target according to manufacturer calibration for the whole spectral range (Labsphere). Remote sensing reflectance is calculated by the following equation: $R_{rs} = (L_t - \rho*L_{sky})/E_d$, where ρ is the sea surface reflectance factor. Values of $\rho = 0.021$ to 0.028 were considered and will be given together with the processed data. For each station, the averages of all individual scans for L_t, L_{sky} and L_d were taken into account and used in R_{rs} calculations. Since all measurements were carried out in clear and "light" coastal waters (waters with small turbidity where the reflectance signal at 750 nm can be still considered close to 0), $R_{rs}(750)$ was subtracted for the entire R_{rs} spectrum to eliminate sunglint effects [*Mobley*, 1999]. Integration time is self-adjusted by the instrument and was typically 160 ms for water observations.

The ASD HandHeld2 instrument is the same as used by other groups. Measurement and processing methodologies were similar to those described for GER with the substantial difference being that the "optimization" procedure is required for each target which adjusts the integration time varied for water observations in the range 6 ms to 4000 ms. The instrument was purchased in 2013 when it was calibrated for the lens mode.

The HyperSAS-POL instrument from the Long Island Sound Coastal Observatory (LISCO) platform was used for the operation from the bow of the ship and has undergone significant modifications which include: (1) complete modification of the instrument platform for attachment to the forward mast of the research vessel; (2) development of the software, electronics and communication systems for continuous (underway) positioning of the HyperSAS-POL at 90° or 135° from the Sun (depending on ship orientation) for the sun glint minimization; (3) installation of additional radiometric sensors for polarimetric observations of the sky; and (4) incorporation of a tilt sensor for exact knowledge of sensor geometry with respect to the ocean. Photos of the HyperSAS-POL on the forward mast of the ship are shown in Fig. 17. The instrument was used in a similar mode during the NASA Ship-Aircraft Bio-Optical Research (SABOR) cruise (July to August 2014). Additional modifications were made for operations on NOAA Ship *Nancy Foster*. The instrument contains 3 HyperOCR sensors (Satlantic) with 3° FOV looking at the water with ≈40° viewing angle from nadir (1 sensor is unpolarized, 1 sensor with horizontal polarization, and 1 sensor with 45° polarization) and 3 similar sensors for the sky observations. An E_d irradiance sensor was positioned in the unobstructed area on the railing of the ship. In cases when our sensor was shadowed by ship's superstructure, E_d data from Zibordi's JRC group was used. In the

unpolarized mode the remote sensing reflectance spectra were determined in the manner similar to the one described above for GER instrument with E_d irradiance used instead of L_d from the plaque. For the polarized mode, processing is very complex and currently under study. Integration time is self-adjusted by the instrument and was 2000 ms for water observations. Data were collected every 2 s during the daytime. Multiple R_{rs} spectra collected for each station were averaged.

Comparison of spectra measured by HyperSAS and GER with VIIRS and MODIS satellite data for Stations 3 (clear water) and 23 (coastal) are shown in Fig. 18 demonstrating the potential of the HyperSAS instrument for accurate above water observations.

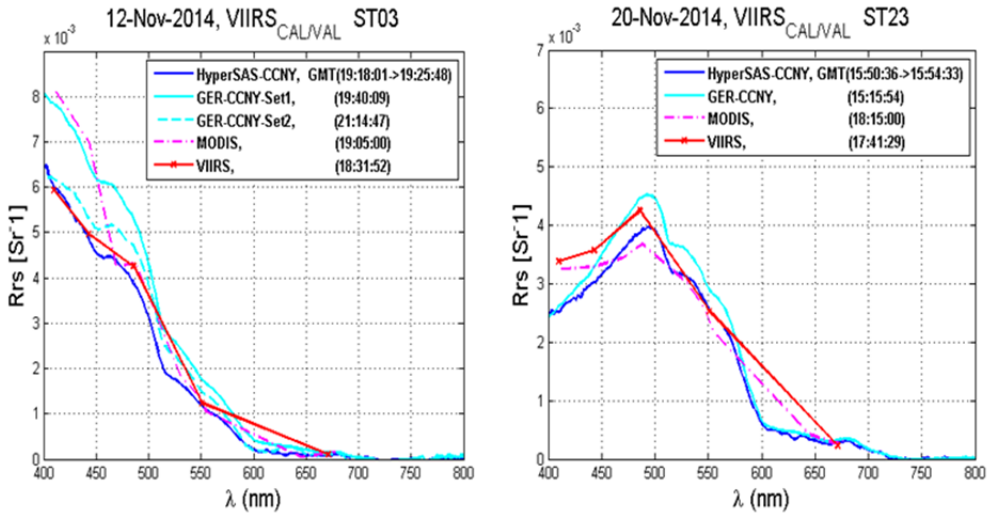

Figure 18. Comparison of measured spectra with satellite data. X-axis is wavelength.

An ECO BB3 instrument (WET Labs) to measure backscattering coefficients was installed as a part of the flow-through system. The instrument was placed into the special chamber (Sequoia Scientific, WA), for underway measurements [*Dall'Olmo et al.*, 2009]. Sensor calibration was provided by WET Labs. Backscattering coefficients were measured at 3 wavelengths: 469 nm, 529 nm and 652 nm.

7.7. Stennis (USM and NRL) – Robert Arnone, Wesley Goode, Sherwin Ladner and Ryan Vandermeulen

Stennis participation and measurements on the cruise included: 1) IOPs from flow-through; 2) above water ASD; 3) floating HyperPro and 4) aerosol optical thickness (AOT). These measurements and the methods used for collection and processing are documented here for the Stennis Cal/Val team from University of Southern Mississippi and the Naval Research Laboratory.

1) IOP Flow-through System on the *Nancy Foster*

IOPs were measured continuously on the cruise using two ac-9 (absorption, and beam attenuation/scattering) instruments connected to the ship's flow-through system. These measurements address cruise objectives to:

a. Characterize the spatial variability of water's optical properties and how the variability impacts the uncertainty of in situ measurements used for VIIRS calibration and validation.
b. Define Gulf Stream processes associated with frontal boundaries and the validation of VIIRS ocean color to define these processes, and characterize the response of the ocean's optics to plankton functional groups and optical water mass classification.

The ac-9 instrument measures the spectral beam attenuation ($c_t(\lambda)$) and the total absorption ($a(\lambda)$) at nine wavelengths which cover the visible to near infrared (412 nm, 440 nm, 488 nm, 510 nm, 532 nm, 555 nm, 650 nm, 676 nm, 715 nm). The spectral scattering ($b(\lambda)$) can be determined from the difference, i.e., $b = c - a$. [*Leymarie et al.*, 2010; *Zaneveld et al.*, 1994].

The instruments (serial numbers: 132 and 243) were interfaced with the ship's flow-through system which pumped water from a water depth of ≈3 m. The ac-9 instruments were used for their known stability and accuracy. This is important in order to correctly address the scattering correction that must be applied [*WETLabs*, 2011; *Zaneveld et al.*, 1994].

The ac-9 protocols for data collection and processing were used and are considered standard. One of the flow-through ac-9 systems (non-filtered) was used to measure the "total" IOPs, which includes both the particles and the dissolved gelbstoff properties of the waters sampled. A second ac-9 system (filtered) used a filtered water input from a Cole Palmer 0.2 μm filter to remove the particles so that the IOPs from the dissolved fraction were determined. The filtered ac-9 is used to determine the spectral absorption and scattering associated with the colored dissolved organic matter (CDOM; i.e., gelbstoff). The difference between the unfiltered and filtered ac-9 instruments provides the spectral absorption and scattering directly associated to particles [*Twardowski and Donaghay*, 2001; *Twardowski et al.*, 1999]:

$$a_p(\lambda) = a_g(\lambda)(non-filtered) - a_{pg}(\lambda)(filtered) \qquad (9)$$

where absorption constituents from particles (a_p) can be determined from the difference of total absorption (a_{pg}; non-filtered) and absorption of gelbstuff (a_g; filtered).

To ensure stability and reliability, the ac-9 instruments were placed in a temperature-stabilized water bath to dissipate the instruments' heat and maintain a constant temperature (Fig. 19). This is critical because temperature instabilities impact the scattering and absorption measurements. The instruments had warm up time at the set temperature to allow them to stabilize and measure consistently. This was confirmed in the calibration results yielding consistent values.

The two ac-9s were interfaced with a WET Labs DH4 data logger with additional inputs from 1) the ship's flow-through system and 2) the backscattering sensor from CCNY.

The ship's flow-through data inputs included position, time, date, heading, water temperature, salinity, and fluorescence (voltage). These inputs were required for the standard protocol corrections during the post processing of the ac-9 data.

The DH4 Host software was used to store these data inputs and displayed in real-time using the WetView software application during data collection. The spectral absorption and beam attenuation were displayed in real time to evaluate the ac-9 data and ensure the systems were operating correctly and producing reliable and consistent data. The data sample rate of the ac-9s was 6 Hz for the duration of the cruise. This equates to a spatial resolution of ≈10 m at ship velocity of 5 knots. Data files from the DH4 were saved hourly for the entire cruise.

The ac-9 instruments were calibrated 4 times: 1) once prior to the cruise; 2) twice during the cruise on 14 and 19 November 2014 and 3) once after the cruise. Calibration of the ac-9 included running Nanopure water through the ac-9 systems using a gravity feed as the instruments were allowed to stabilize for some time interval (≈5 min to ≈10 min). The calibration procedure included obtaining the clear water calibration before and after cleaning the absorption and scattering tubes. An update to instrument device files was applied in real-time if it was deemed that new corrections were necessary to assure good quality measurements.

Figure 19. IOP setup shows water bath setup used for the ac-9 instrument. The ac-9s are located inside the PVC containers and were in a constant temperature water bath during operation.

Post processing of the ac-9 data followed the "WET Labs, 2011" protocols. The ac-9 data were processed using a scattering correction [*Zaneveld et al.*, 1994], removing of the absorption of gelbstuff (a_g) and adding back the pure water absorption [*Pope and Fry*, 1997]. Additionally, the water absorption corrections for temperature and salinity were applied for ac-9 processing using the ships flow-through data following [*Pegau et al.*, 1997; *Sullivan et al.*, 2006]. This is required to account for the large changes between coastal and open ocean waters.

The standard order of post processing steps used include:

- Temperature and salinity corrected measured (in situ) absorption (a) and beam attenuation (c)
- Temperature correct pre- and post- pure water calibration data, absorption (a) and beam attenuation (c)
- Subtract pure water calibration data from in situ data
- Omit spikes in data due to bubbles, etc. using a standard deviation filter, then interpolate
- If filtered ac-9 meter (CDOM) exists, then compute $a_p = a_t - a_g$
- Apply scatter correction [*Zaneveld et al.*, 1994] to a_p
- If filtered ac-9 meter (CDOM) exists, then add scatter corrected a_p back to a_g to yield $a_{t\text{-}w}$.
- Add spectral pure water absorption coefficients [*Pope and Fry*, 1997] to $a_{t\text{-}w}$ to yield a_t.
- Compute spectral scattering $b = c_t - a_t$
- Compute spectral omega = b/c

The ac-9 flow-through data is being processed to identify the spatial coherence of the IOPs and to detect important features and water mass changes for further investigation. The ac-9 data will be merged with the ship flow-through data using the WET Labs WAP software to combine datasets. This merged dataset will be used to characterize the spatial variability of changing water optical properties. The WAP-combined dataset will be used to define the spatial coherence scales from the IOP data during transitions among multiple ocean fronts in the Gulf Stream and shelf regions. The real time IOPs from the flow-through were used to determine station locations and interesting features during the cruise. These changes in the IOPs were clearly associated with the temperature and salinity changes as the Gulf Stream was transected. The VIIRS ocean color products of backscattering (at 551 nm) and chlorophyll were used to adaptively modify the cruse track and validated using the flow-through IOPs system.

The flow-through data will also be used to determine the variability of the IOPs with respect to the changing water masses observed at each of the 23 stations. Continuous monitoring of the IOPs while on stations from start to end can account for the changing water masses during shipboard data collection due to station drift. This can be significant especially during stations at frontal boundaries with high variability. We will examine how the IOPs changed during the duration of the stations to help define how IOP variability contributes to the uncertainty in the water-leaving radiance measurements from the HyperPro and the ASD and also allow for better matchups between radiometric, IOPs and satellite measurements.

The ac-9 flow-through will be used to characterize the spectral differences in the IOPs of water masses. The changes in the particle and CDOM properties in upwelling and downwelling regions of the Gulf Stream will be identified so that the ocean color response (e.g., sensitivity of nL_w to these properties) can be estimated. The changes in the IOPs result from the packaging and composition of the particles and the distribution of organic and mineral components. We will link the IOPs and particle composition with the FlowCam measurements (by LDEO) to investigate and identify the changes in the phytoplankton functional groups including particle shape, size and absorption.

The flow-through system will provide an extensive data set from a large variety of the water masses and ocean processes that were identified on the cruise track. The ac-9 flow-through data will provide an opportunity to validate the VIIRS ocean color IOPs products by examining the along track matchup. Additionally, the high spatial resolution of the flow-through can be used to validate the VIIRS 750 m matchup from a weighted average of the in situ measurements.

2) Above water ASD Measurements

Above-water remote sensing reflectance measurements were taken using multiple ASDs (PANalytical) FieldSpec Spectroradiometers with two similar instruments from USM and NRL (Fig. 20). These instruments enable the derivation of above-water R_{rs} using un-calibrated radiance relative to reflectance plaque measurements. The reflectance plaque is a 10 % gray card with a known BRDF and is assumed to be a semi-Lambertian surface. The field collection protocols are described as follows.

Using a 10° fore-optic attachment, five consecutive radiometric spectrum (S) measurements were taken of each of the following targets: Gray card (S_g), water (S_{sfc}), and sky (S_{sky}). Prior to measuring each individual target, the ASD instrument was manually re-optimized (i.e., integration time of sensor was changed based on relative brightness of the target and new dark counts were taken to correct for instrument noise). Integration times ranged from 68 ms to 4352 ms. Most measurements were taken from the stern of the ship. The exact location of sampling (port vs. starboard) was dependent on the orientation of the ship relative to the sun to eliminate shadowing from the vessel. The optical sensor zenith angles for the water (θ_{sfc}), gray card (θ_g), and sky (θ_{sky}) measurements were 135°, 135° and 45°, respectively. The relative azimuth angle of the sensor to the sun ($(\Delta\varphi)$) was > 90°, but may have been adjusted up to 135° depending on sea foam resulting from the ship's wake.

Figure 20. Ryan Vandermeulen and Robert Arnone (USM) aboard the NOAA Ship *Nancy Foster*, taking above-water radiometric measurements of a gray plaque using an Analytical Spectral Device (ASD) HandHeld Spectroradiometer. The gray plaque has a known BRDF and is used to normalize the un-calibrated radiance measurements to E_S.

The processing protocols for deriving R_{rs} from above water radiometry follow method 2 of Chapter 3 of Mueller et al. [2003]. To compute R_{rs}, we first obtain the sensor response signal, S, from n readings from each target and normalize to the same consistent integration time (1 sec):

$$S = \frac{\int_{i=0}^{n} CI_N/I_i}{n} \tag{10}$$

Here, C represents the un-calibrated data read from the instrument, I_i is the integration time used for that reading, I_N is the normalized (to 1 s) integration time, and n is the number of readings (3, 5, or 9 in practice depending on instrument protocol).

Following Chapter 2 of the Optics Protocols [*Mueller et al.*, 2003], one can express the water-leaving radiance, L_w, and incident spectral irradiance, E_S, in these terms:

$$L_w = F_L \left[S_{sfc} - \rho S_{sky}\right], E_S = \frac{\pi F_L S_g}{R_g} \tag{11}$$

Here, F_L is the unknown instrument radiance response calibration factor (which will cancel when calculating R_{rs}) and R_g is the gray plaque's bi-directional reflectance function. The R_{rs} can be computed from the un-calibrated data using the following equation (correcting sky using Fresnel reflectance ρ of 0.021):

$$R_{rs}(\lambda) = \frac{S_{sfc}(\lambda) - \rho S_{sky}(\lambda)}{\pi S_g(\lambda) - R_g(\lambda)} \tag{12}$$

The computed R_{rs} should be "black" at about 750 nm. If not zero, then it is assumed that the reflected skylight term (S_{sky}) was not estimated correctly. Following the "quick and easy" algorithm of Carder and Steward [1985], it is further assumed that any error in the skylight reflection term is white (not wavelength dependent) and one may simply subtract the computed $R_{rs}(750)$ from the entire spectrum. In

practice, this may lead to negative values of R_{rs} near 750 nm. Therefore, the processing subtracts the smallest R_{rs} in the range from 700 nm to 825 nm.

$$R_{rs}(\lambda) = R_{rs}(\lambda) - MIN\left(R_{rs}(700\ to\ 825)\right) \quad (13)$$

To compare the in situ reflectance with satellite-derived reflectance, the mean reflectance is computed using the relative spectral response tables for each band of the satellite (VIIRS) data.

Slightly modified equations were used to derive the relative reflectance of the blue tile (R_{tile}). For the blue tile measurements, the derived reflectance is simply expressed as the ratio of the radiance (or net signal) for the test target (S_{tile}) to the standard gray target.

$$R_{tile}(\lambda) = R_g(\lambda)\frac{S_{tile}(\lambda)}{S_{ref}(\lambda)} \quad (14)$$

The Stennis team collected ASD spectroradiometer data at all 23 stations. These data were processed using NRL processing.

ASD – Multiple instruments and blue tile comparisons - There were multiple sensors collecting data at each station, making for a sum total of 106 total ASD measurements between the five participating institutions (USM and NRL of the Stennis group, USF, CCNY and NOAA/STAR). Contemporaneous measurements (at least four ASD instruments at one time) of the water were made at 11 different stations in order to compare variations between the above-water measurements.

To assess the differences among instruments at determining R_{rs}, the relative reflectance of a reference 16.5 cm blue glass tile developed by NIST was measured by the four ASDs identified above. The groups all used the same protocols described above to measure the relative reflectance of the target, using the S_{tile} in place of S_{sfc}. Blue tile comparisons were performed at four different times during the cruise under varying cloud cover conditions (0 % to 40 %). A preliminary analysis revealed that there are nine stations with limited or absent cloud cover where a direct comparison with VIIRS-retrieved R_{rs} is possible.

3) Floating HyperPro measurements

The Floating HyperPro is a hyperspectral profiling radiometer that simultaneously measures above-water downwelling irradiance (E_s) and in-water upwelling radiance (L_u) on a fixed floating platform. The spectral range of both E_s and L_u sensors is from 350 nm to 800 nm, with 10 nm ± 0.3 nm resolution. This instrument was used with a molded floatation collar, enabling in-water surface measurements to be taken over time. The downwelling E_s sensor uses a cosine collector and is approximately 30 cm above the water surface. The upwelling (L_u) radiance sensor is mounted approximately 30 cm below the water surface. While in-water measurements have the advantage of avoiding surface-reflected light, there is a slight influence of self-shading [*Lee et al.*, 2013].

The Floating HyperPro, equipped with a floatation collar, was deployed over the stern of the vessel (Fig. 21). The tether was let out a sufficient distance from the boat (20 m to 30 m), allowing the instrument to float away from the boat. This ensured there was no contamination from vessel-generated bubbles, shadowing, or other potential disturbances. Once the instrument was a sufficient distance from the vessel, data was recorded for 20 min to 30 min. During post-processing, the data are averaged over this deployment interval.

The processing protocols for deriving R_{rs} from in-water radiometry follow Chapter 2 of Mueller et al. [2003]. Water-leaving radiance (L_w) is computed as for Eq. 5 above, but where $\rho = 0.025$ is the Fresnel

reflectance of the air sea interface, and $n = 1.34$ is the refractive index of seawater. Remote sensing reflectance (R_{rs}) is computed as for Eq. 8 above.

Floating HyperPro data were collected at 20 stations. A preliminary analysis revealed that nine stations had limited or absent cloud cover where a direct comparison with VIIRS-retrieved R_{rs} is possible.

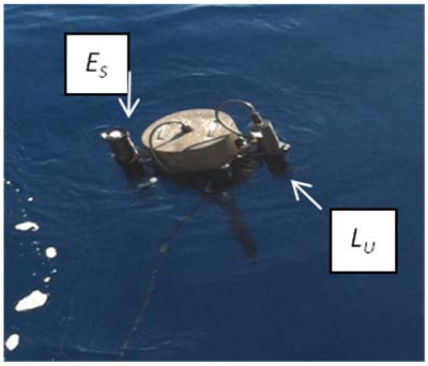

Figure 21. Deployment of the floating HyperPro package

4) Microtops measurements

The Microtops II instrument is a sunphotometer that enables the derivation of aerosol optical thickness (AOT) and water vapor content in the atmosphere. The characterization of these atmospheric components supports the atmospheric correction of satellite data. There are five spectral filters on the instrument (λ = 440 nm, 675 nm, 870 nm, 936 nm, 1020 nm), each with a 10 nm ± 1.5 nm bandwidth. The position and time are required along with the measurements. The instrument is based on knowing the spectral irradiance at the top of the atmosphere and any loss or decrease in direct solar irradiance is attributed to aerosols and molecular scattering and through a given path atmospheric length for the position and time [*Porter et al.*, 2001]. Equipped with a 2.5° FOV, the Microtops II instrument is pointed directly at the sun for several seconds. The measurements require that the sun is visible and not cloud covered.

Microtops data were collected at 12 stations (2 to 4, 10 to 12, 17 to 19 and 21 to 23). In order to characterize the variability of atmospheric components (aerosols) throughout the day, several measurements were taken every hour while on station, making for a sum total of 31 measurements during the cruise (see Appendix A, Table A-2).

7.8. LDEO – Joaquim I. Goes, Helga do Rosario Gomes, Alex Chekalyuk and Kali McKee

Phytoplankton community composition, size structure and photosynthesis competency measurements

Discrete Samples:

At each station (as indicated in Appendix A, Table A-3) aliquots of seawater samples from three depths (coincident with sampling for HPLC pigments) were collected for the following:

i) Microscopic analysis of phytoplankton community composition and sizes.
ii) Counting, imaging and size estimations of phytoplankton and other detrital particles using a Fluid Imaging Technologies, Inc., FlowCam.
iii) Estimates of phycobilipigments using a newly developed fluorescence technique developed at LDEO by Gomes et al. [in prep].
iv) Fluorescence based estimates of
Chl-*a*
CDOM

Phycobilipigments: Phycoerythrin-1 (PE-1; peak at 565 nm), Phycoerythrin-2 (PE-2; peak 578 nm) and Phycoerythrin-3 (PE-3; peak at 590 nm)
and variable fluorescence (Fv/Fm, a measure of phytoplankton photosynthetic competency) using a WET Labs Advanced Laser Fluorometer (ALF) [*Chekalyuk and Hafez*, 2008; *Chekalyuk et al.*, 2012; *Goes et al.*, 2014a]

v) Measurements of (Fv/Fm) and the functional absorption cross-section of Photosystem II (σPSII) in a mini-Fluorescence Induction and Relaxation (FIRe)® Fast Repetition Rate Fluorometer (FRRF) [*Gorbunov and Falkowski*, 2004].

i. Microscopy based phytoplankton identification and cell counts

For microscopic identification and enumeration of phytoplankton, samples were collected in 100 mL screw top hard plastic bottles from three depths and at 27 stations (coincident with HPLC pigment analysis). Samples were fixed with 1 % alkaline Lugol's iodine, preserved in 1.5 % buffered formaldehyde solution and were stored under dark and cool conditions. Microscopic analysis is currently underway and includes overnight settling of 10 mL samples in an Ultermohl counting chamber and then counting the samples using a Nikon® inverted microscope at 200X and 400X magnifications. The smallest cells that can be enumerated by this method are <5 µm in diameter. Phytoplankton identifications are based on standard taxonomic keys [*Tomas*, 1997]. Cryptophytes are being identified by epifluorescence microscopy using their yellow-orange fluorescence signatures [*Booth*, 1993; *Goes et al.*, 2014b; *MacIssac and Stockner*, 1993].

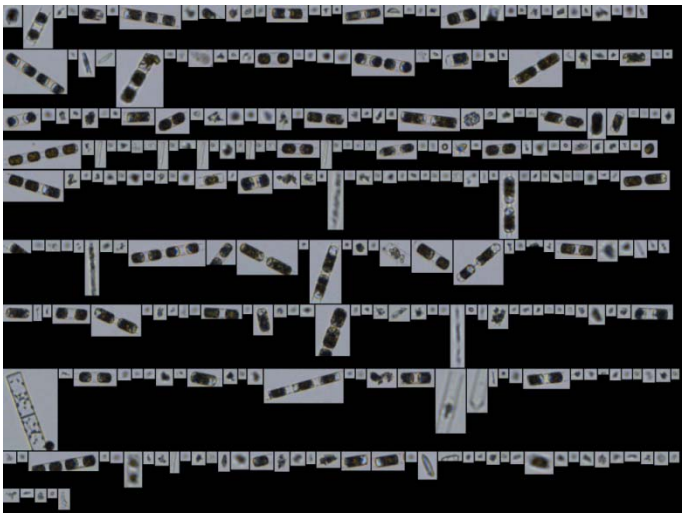

Figure 22. Collage showing the diversity of phytoplankton communities imaged by the FlowCam at a coastal location along the cruise track.

ii. FlowCam based phytoplankton identification, cell counts and cell sizes

In addition to the microscopic analysis of phytoplankton, 2 × 25 mL aliquots of the preserved samples are being analyzed for phytoplankton community composition and size structure analysis using a FlowCam particle imaging system equipped with a 4X objective (UPlan FLN, Olympus®) and a 300 µm Field-of-View flow cell. Field-of-View flow cells ensure that the liquid passing through the flow cell is entirely encompassed within the camera's field of view. Phytoplankton cells within the preserved samples will be counted and imaged in auto-image mode with a peristaltic pump rate of approximately 0.32 mL min^{-1} to 0.44 mL min^{-1} as specified by the manufacturer. Cells will be classified to the genus-level using the Visual Spreadsheet program (v. 2.2.2, Fluid Imaging). The instrument provides the total number of particles imaged, together with the dimensions of each particle allowing estimations of phytoplankton

community structure, particle size distribution of both phytoplankton and of detrital particles (Figs. 22 and 23).

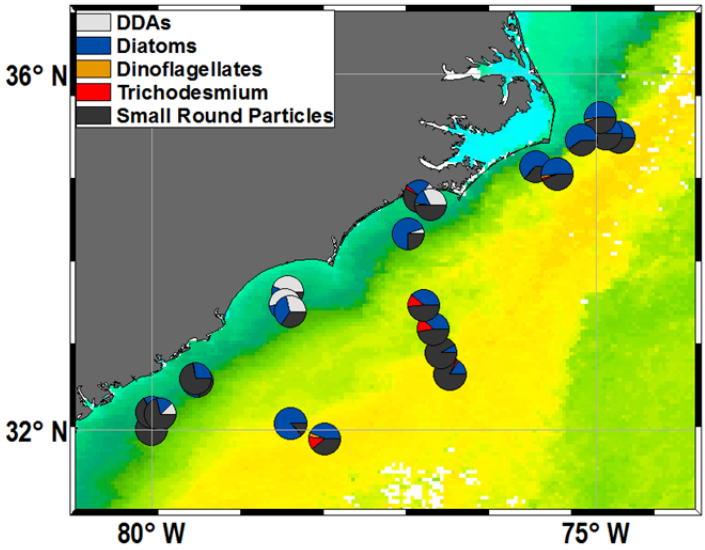

Figure 23. Distribution of major phytoplankton groups in surface samples at discrete sampling stations along the cruise track as measured with the FlowCam.

iii. Phycobilipigment collection and analysis

Approximately 1 L to 2 L of seawater samples from three depths (coincident with the depths sampled for HPLC pigment analysis) were carefully filtered on to 4 × 25 mm Whatman GF/F, glass microfiber filters for analysis of estimating phycoerythrin and phycourobilin pigments. Samples were immediately stored in liquid nitrogen for later analysis at LDEO using methods developed by Gomes et al. [in prep] which rely on freezing, sonication and extraction of the phycobilipigments in phosphate buffer and analysis in a spectrofluorometer.

iv. Automated Laser Fluorescence (ALF) measurements of phytoplankton groups

The ALF combines high-resolution spectral measurements of blue (405 nm) and green (532 nm) laser-stimulated fluorescence with spectral deconvolution techniques to quantify fluorescence of Chl-*a* (peak at 679 nm), three phycobilipigment types (PE-1, PE-2 and PE-3), CDOM (peak at 508 nm) and variable fluorescence (Fv/Fm). All fluorescence values obtained are normalized to the Raman spectra of seawater and generally expressed as relative fluorescence units (RFU), whereas Fv/Fm is unitless. PE-1 type pigments are associated with blue water or oligotrophic cyanobacteria with high phycourobilin/phycoerythrobilin (PUB/PEB) ratios, PE-2 type phytoplankton with low-PUB/PEB ratios are generally associated with green water cyanobacteria that usually thrive in coastal mesohaline waters, and PE-3 attributable to eukaryotic photoautotrophic cryptophytes [*Chekalyuk and Hafez*, 2008; *Chekalyuk et al.*, 2012; *Goes et al.*, 2014b]. RFU values for Chl-*a* can be converted into mg m^{-3} Chl-*a* values using least square regressions of acetone or HPLC measured Chl-*a* with RFU values for Chl-*a* measured in an ALF.

All samples for the ALF were collected directly from the Niskin samplers into 500 mL acid-washed amber glass bottles and stored for about 30 min in the dark at temperatures close to the average surface seawater temperature at each station. Dark adaptation allows all of the PSII reaction centres and electron acceptor molecules of phytoplankton to become fully oxidised and hence available for photochemistry thus minimizing the impacts of non-photochemical quenching before analysis. Figure 24 shows preliminary flow-through data from ALF.

v. Fluorescence Induction and Relaxation (FIRe) measurements of photosynthetic competency

The FIRe technique was developed to measure a comprehensive suite of photosynthetic and physiological characteristics of photosynthetic organisms [*Bibby et al.*, 2008; *Gorbunov and Falkowski*, 2004]. This technique provides a set of parameters that characterize photosynthetic light-harvesting processes, photochemistry in Photosystem II (PSII), and the photosynthetic electron transport down to carbon fixation (see Fig. 25 for example of flow-through FIRe data). Because these processes are particularly sensitive to environmental factors, the FIRe technique can be utilized to provide a measure of natural (nutrient limitation, photoacclimation and photoinhibition, thermal and light stress, etc.) and anthropogenic stressors (such as pollution). One property that is unique and the most sensitive to environmental stressors is Fv/Fm. All optical measurements by the FIRe are sensitive, fast, non-destructive, and can be done in real time and in situ and can provide an instant measure of the photosynthetic competency of the cells.

Underway flow-through measurements:

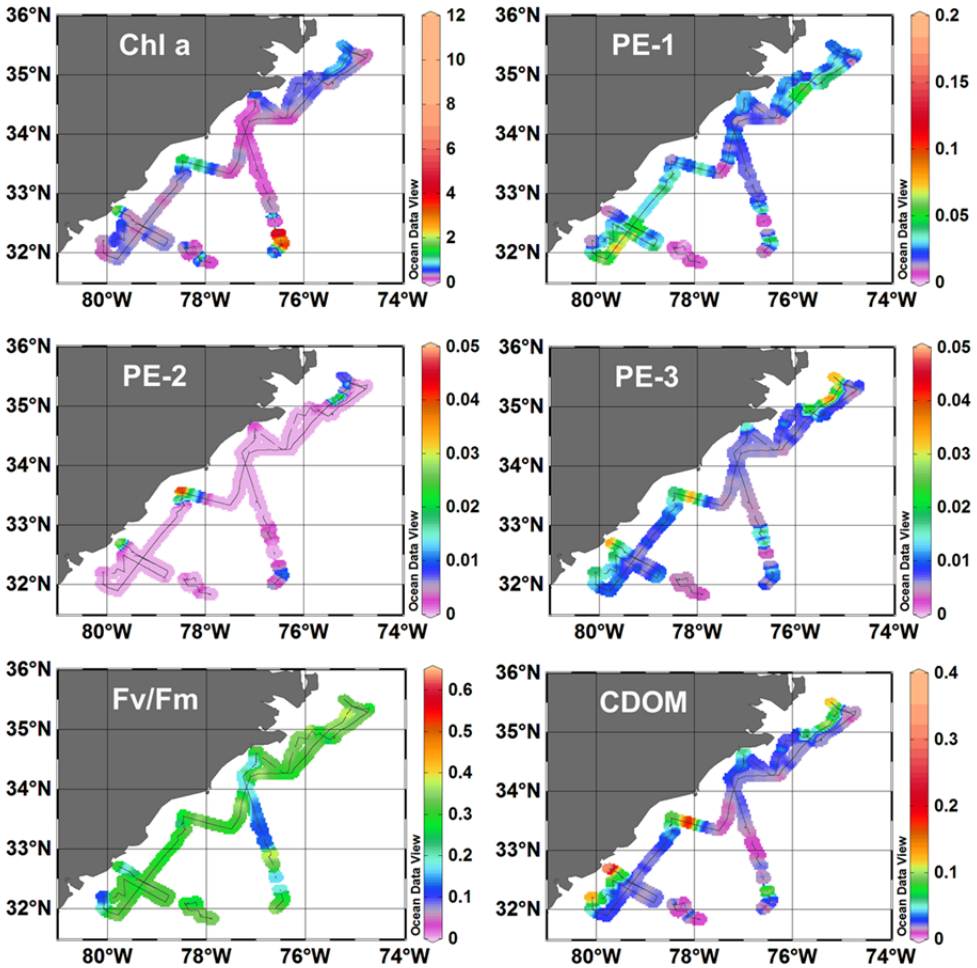

Figure 24. Preliminary analysis of flow-through ALF data along the cruise track showing the distribution Chl-*a*, Phycobilipigments (PE-1, PE-2 and PE-3) measured as Relative Fluorescence Units (RFU), variable fluorescence (Fv/Fm; dimensionless) and CDOM (RFU).

Between stations, the ALF, the FlowCam, the mini-FIRe and a bbe Moldeanke AlgaeOnlineAnalyser [*Richardson et al.*, 2010] were connected in parallel to the ship's seawater flow-through system, allowing for continuous in-water measurements of phytoplankton community composition, phytoplankton size, phycobilipigment types and photosynthetic competency. With the exception of a few breaks during stations and for reconditioning, all four instruments were operated over the entire cruise track shown in Figs. 21-26), providing several thousand fluorescence based measurements of Chl-*a*, CDOM, PE-1, PE-2, PE-3, Fv/Fm and σPSII as well as continuous FlowCam images that will allow high resolution measurements of phytoplankton composition and cell size distribution necessary for interpreting the optical measurements inside and outside of the Gulf Steam filaments and meanders, in the coastal and in the open ocean waters. The AlgaeOnlineAnalyser allows for continuous measurements of Chl-*a*, plus determination of cyanobacteria, green algae, brown algae (diatoms and dinoflagellates) and cryptophytes fluorescence using colored light emitting diodes.

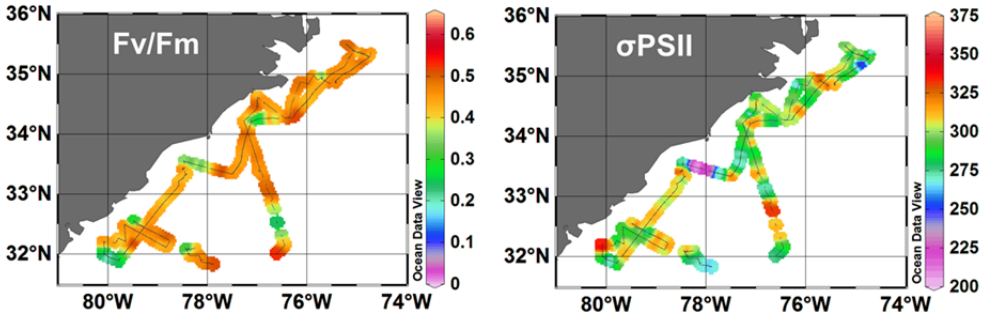

Figure 25. Preliminary analysis of flow-through data measured by the mini FIRe showing photosynthetic characteristics, Fv/Fm (dimensionless) and σPSII ($Å^2$ $quanta^{-1}$) of phytoplankton populations along the cruise track.

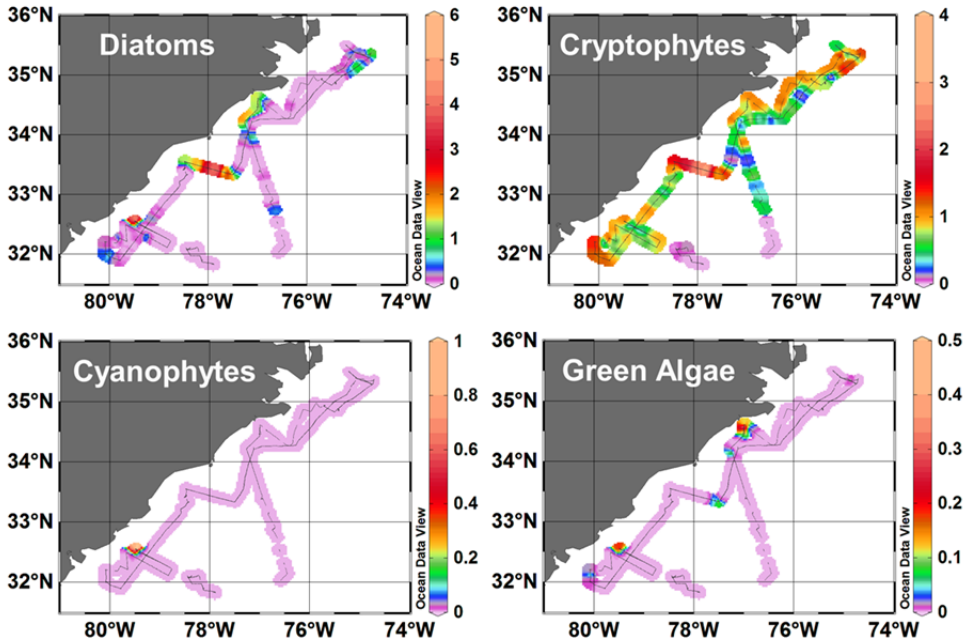

Figure 26. Preliminary analysis of AlgaeOnlineAnalyzer flow-through data showing distribution of major phytoplankton groups along the cruise track. All values are in µg L^{-1}.

7.9. NASA/GSFC – Scott Freeman and Aimee Neeley

The overarching goal of the NASA Goddard Field Support Group is ensuring and expanding the ability of the research community to generate complete sets of in situ optical and biogeochemical data for inclusion in Earth science climate data records and other supporting data records used for ocean color satellite vicarious calibration, data product validation, and bio-optical algorithm development. For all biogeochemical parameters described below, water from three hydrographic depths (bottom, mid depth and surface) from each CTD rosette cast was transferred from the Niskin bottles to 10 L carboys. The carboys were covered with black plastic bags to prevent high light exposure. HPLC pigments are used to characterize the phytoplankton community at each station and will be compared to the FlowCam data. Additionally, collection of organic carbon (POC, CDOM, DOC) provides a greater understanding of regional carbon sequestration and cycling. The total numbers of samples collected for each parameter are shown in Table 3.

Biogeochemical parameters from water samples

HPLC Pigments
Discrete samples from three depths were collected for analysis by HPLC to quantify Chl-*a* and other pigments diagnostic of phytoplankton groups. For each sample, a measured volume of water was filtered under gentle vacuum (≈127 mm Hg) through a polysulfone filter apparatus onto a Whatman GF/F filter (nominal pore size ≈0.7 μm), wrapped in a pre-cut foil pouch and flash frozen in liquid nitrogen. Filters from the surface and mid depth were collected in duplicate for most samples. One filter was collected from the bottom depth. The samples were stored at -80°C until analysis by Crystal Thomas and Chris Kennemer at NASA Goddard Space Flight center using a method modified from [*Van Heukelem and Thomas*, 2001].

Colored Dissolved Organic Matter (CDOM)
Discrete samples from surface and mid depth were collected for determination of CDOM spectral absorption coefficients. The samples were filtered under gentle vacuum (≈127 mm Hg) either through 0.2 μm Whatman Nucleopore polycarbonate filters (open ocean) or through pre-combusted 47 mm diameter GF/F filters (coastal waters) using a pre-combusted glass filtering apparatus into pre-cleaned, pre-combusted 250 mL glass amber bottles. The samples were then stored under refrigeration. In the laboratory, CDOM samples will be warmed to room temperature and filtered through 0.2 μm Whatman Nuclepore polycarbonate filters or Gelman Supor (polyethersulfone) filters prior to analysis [*Mitchell et al.*, 2000]. Absorption spectra of CDOM will be measured using a UV-Visible scanning spectrophotometer (250 nm to 800 nm) with UV oxidized Milli-Q water as the blank and reference [*Mannino et al.*, 2008; *Mitchell et al.*, 2003].

Dissolved Organic Carbon (DOC)
Discrete samples for DOC were collected in duplicate similarly to CDOM except that the filtrate was collected into pre-cleaned, pre-combusted amber glass vials. Samples were stored frozen (-20°C) until analysis. DOC samples will be measured by high temperature combustion oxidation using a Shimadzu TOC-V. The instrument will inject each sample up to seven times until 3 of those samples have a confidence value of < 2 %. [*Benner and Strom*, 1993; *Mannino et al.*, 2008; *Sharp et al.*, 2002]. The deep Sargasso Sea water or Florida Straight water certified reference material (Hansell Laboratory, University of Miami RSMAS) will be used daily to verify the accuracy of DOC measurements and maintain an analytical uncertainty to within ±5 %.

Particulate Organic Carbon and Particulate Nitrogen (POC/PN)
Discrete samples from the surface and mid depth were filtered in duplicate onto pre-combusted (6 h at 450°C) Whatman GF/F 25 mm filters using a clean glass filtering apparatus. The filters were collected in duplicate for surface and mid depth samples, stored in pre-combusted foil pouches and flash frozen in

liquid nitrogen. In the laboratory, the samples are stored at -80°C until analysis. Prior to analysis, the filters will be dried for ≈48 h in a drying oven at 45°C to 50°C. POC samples will then be placed overnight in a sealed desiccator saturated with hydrochloric acid fumes (i.e., 0.012 mol m^{-3} HCl, or 12M HCl as more commonly expressed) to remove inorganic carbon from samples for ≈24 h [*Hedges and Stern*, 1984]. Acidified filters will be dried again as described previously and packed into tin foil sheets for analysis. POC, PC and PN will be measured using an elemental analyzer.

Table 3. Biogeochemical parameters collected by NASA/GSFC.

Parameter	Number of samples collected
HPLC Pigments	102
POC/PN	90
a_{CDOM}	46
DOC	92

In-Water Optical Measurements (AOPs, IOPs)

The instrument package to measure IOPs was equipped with two attenuation and absorption spectrometers (one ac-s and one ac-9; WET Labs). The ac-9 was equipped with a 0.2 μm pre-filter to enable the in situ measurement of a_g. The IOP package also included two scattering meters (ECO BB9 and VSF-9; WET Labs), and a Sea Bird SBE 49 CTD. The ac-s and ac-9 meters measure absorption and attenuation (and total scattering by difference) at 74 and 9 wavelengths, respectively, between 400 nm and 740 nm, while the ECO BB9 measures backscatter at 9 wavelengths and 117°. The VSF-9 measures scattering at 9 angles (62°, 76°, 80°, 90°, 110°, 120°, 140°, 160°, 170°) at 532 nm. A 31 A-h Lithium-ion battery pack (Sartek, Inc.), housed in a Sexton, Inc. housing, was used for powering all instruments, and data was stored in a WET Labs DH-4 data handler. The package performed casts of up to 150 m at 21 of 23 stations during the campaign (see Appendix A, Table A-2).

The IOP package was designed such that all instruments are sampling the same depth. The CTD and ac inlets are at the same level as the faces of the scattering instruments. However, with the flow-through ac-9 and ac-s, there is a delay between the water entering the flow tube and the measurement being made. In addition, water entering the ac-9 must also pass through a 0.2 μm filter. To account for this delay, a lag of 1.5 s is added to the ac-s. Because of the strong correlation of absorption and water temperature at 715 nm, the temperature and a_{715} can be compared in order to find the appropriate delay. A MATLAB GUI was used to determine the delay.

The ac-9 and ac-s were calibrated twice during the cruise on 11 and 19 November 2014. Calibrations on the 11th included both water brought from our lab and water purified at sea. No difference was apparent, so locally produced water was used on the 19th. The scattering sensors were calibrated by James Sullivan at WET Labs in Rhode Island on 5 September 2014. Dark-current measurements were collected before the first cast with all pumps and instruments turned on.

In-water AOPs, both downwelling irradiance (E_d) and upwelling radiance (L_u), were measured using a Biospherical Instruments C-OPS system. Incoming solar irradiance (E_s) was measured with an irradiance radiometer. The three radiometers have a spectral range from 300 nm to 900 nm, with 19 wavebands centered at: 305 nm, 320 nm, 340 nm, 380 nm, 395 nm, 412 nm, 443 nm, 465 nm, 490 nm, 510 nm, 532 nm, 555 nm, 565 nm, 625 nm, 665 nm, 683 nm, 710 nm, 780 nm and 875 nm. The upwelling radiance radiometer substitutes a broad natural chlorophyll fluorescence sensor (27 nm FWHM, centered at 683

nm) for the 875 nm sensor. All other wavelengths are 10 nm FWHM. The radiometers feature three gain stages, which provide nine decades of dynamic range [*Morrow et al.*, 2010].

Before each deployment, dark current measurements at each of the three gain stages and a pressure tare were made on deck by capping the sensors and running the dark current procedure through the μProfile software (C-OPS manual). The C-OPS system was deployed at each station, with over 200 profiles in total. Each radiometer was calibrated at NOAA NESDIS, College Park before and after the cruise. Prior to the cruise calibration, the system was calibrated at the manufacturer's facility in January 2014.

Above-water AOPs (E_s, L_{sky}, L_t) were measured using a Satlantic HyperSAS system. This had a newly-developed solar-tracking system, but the system unfortunately didn't work during the cruise because of a malfunction in the motor assembly. After the first two days of attempted setup, we decided to use it as a stationary instrument, setting it 90° to port, such that when the sun was directly ahead or astern the radiometers would be at the proper angle to the sun. We found that when the sun was astern, the system was often in shadow due to the low solar altitude and the ship's superstructure. After noticing this, a procedure was developed to maneuver the ship before and after each station to collect data with the sun ahead.

The above-water radiometers were calibrated at Satlantic's calibration facilities before the cruise in August 2014, and were also calibrated at NOAA/STAR, College Park afterward. The hyperspectral radiometers have a spectral range of 305 nm to 1150 nm, and were calibrated for the full range.

8. Conclusion

The 2014 VIIRS dedicated Cal/Val cruise aboard the NOAA Ship *Nancy Foster* was successful in achieving all its planned measurement objectives, despite some rough weather and cloudy conditions, thanks to the hard work and dedication of the science team and ship crew. The VIIRS ocean color sensor performance validation data sets were collected on 9 of the 23 stations when clear-sky conditions were encountered during in situ sampling and the satellite overpass. VIIRS-derived normalized water-leaving radiances will be compared to multiple ship board measurements that utilized several techniques. These included profiling, floating and above-water instrumentation from several manufacturers. In addition to the satellite radiance, many derived ocean color products will also be compared. Some of these derived products are chlorophyll-a concentration, absorption and backscattering properties, attenuation coefficients, phytoplankton characteristics and TSM. The uncertainties in the in situ validation measurements will be estimated by utilizing pre- and post-cruise calibrations of instruments, simultaneous measurements of parameters utilizing multiple techniques and instruments and evaluation of data processing techniques. Oceanic processes will be investigated using multiple platform techniques, which include near-real time satellite measurements, in situ flow-through, profiling, and above water data. The Gulf Stream fronts were traversed many times. These strong spatial gradients will be studied using in situ data and compared to VIIRS data to assess the ability of the sensor to capture the scales and magnitude of the naturally occurring variability. In summary, a wealth of high quality in situ data was collected and is being analyzed to provide a comprehensive evaluation of VIIRS performance, validation techniques, and various ocean color applications.

9. Acknowledgments

All data collected on this cruise will be publically available through NOAA CoastWatch repository and will be formally archived according to NOAA guidelines. Data users are strongly encouraged to communicate with cruise investigators for appropriate collaborations and/or citations. Funding for this project was provided as follows: NOAA OMAO for ship time and crew support; JPSS VIIRS Ocean

Color Cal/Val funding. Participating science groups provided their own support. Participants thank the crew of the NOAA Ship *Nancy Foster* for their support in making data collection possible. The views, opinions, and findings contained in this report are those of the authors and should not be construed as an official NOAA or U.S. Government position, policy, or decision.

10. References Cited

Arnone, R. A., D. A. Wiesenburg and K. D. Saunders (1990), The origin and characteristics of the algerian current, *J. Geophys. Res.-Oceans*, *95*(C2), 1587-1598, doi: 10.1029/JC095iC02p01587.

Austin, R. W. (1974), The remote sensing of spectral radiance from below the ocean surface, in *Optical Aspects of Oceanography*, Academic Press.

Benner, R. and M. Strom (1993), A critical-evaluation of the analytical blank associated with doc measurements by high-temperature catalytic-oxidation, *Marine Chemistry*, *41*(1-3), 153-160, doi: 10.1016/0304-4203(93)90113-3.

Bibby, T. S., M. Y. Gorbunov, K. W. Wyman and P. G. Falkowski (2008), Photosynthetic community responses to upwelling in mesoscale eddies in the subtropical North Atlantic and Pacific Oceans, *Deep Sea Research Part II: Topical Studies in Oceanography*, *55*(10–13), 1310-1320, doi: 10.1016/j.dsr2.2008.01.014.

Booth, B. C. (1993), *Estimating cell concentration and biomass of autotrophic plankton using microscopy.*, Lewis Publishers, Boca Raton, Florida, USA.

Carder, K. L. and R. G. Steward (1985), A remote-sensing reflectance model of a red-tide dinoflagellate off west Florida, *Limnology and Oceanography*, *30*(2), 286-298.

Chekalyuk, A. and M. A. Hafez (2008), Advanced laser fluorometry of natural aquatic environments, *Limnology and oceanography, methods*, *6*, 591.

Chekalyuk, A. M., M. R. Landry, R. Goericke, A. G. Taylor and M. A. Hafez (2012), Laser fluorescence analysis of phytoplankton across a frontal zone in the California Current ecosystem, *Journal of Plankton Research*, *34*(9), 761-777, doi: 10.1093/plankt/fbs034.

Clark, D. K., H. R. Gordon, K. J. Voss, Y. Ge, W. Broenkow and C. Trees (1997), Validation of atmospheric correction over the oceans, *Journal of Geophysical Research-Atmospheres*, *102*(D14), 17209-17217, doi: 10.1029/96jd03345.

D'Alimonte, D., G. Zibordi, T. Kajiyama and J. C. Cunha (2010), Monte Carlo code for high spatial resolution ocean color simulations, *Applied Optics*, *49*(26), 4936-4950, doi: 10.1364/ao.49.004936.

Dall'Olmo, G., T. K. Westberry, M. J. Behrenfeld, E. Boss and W. H. Slade (2009), Significant contribution of large particles to optical backscattering in the open ocean, *Biogeosciences*, *6*(6), 947-967.

Dickey, T. D. (1991), The emergence of concurrent high-resolution physical and bio-optical measurements in the upper ocean and their applications, *Reviews of Geophysics*, *29*(3), 413, doi: 10.1029/91RG00578.

EPA (1971), Methods for chemical analysis of water and wastes, EPA-NERL: 160.2, US Environmental Protection Agency, vol.

Gergely, M. and G. Zibordi (2014), Assessment of AERONET-OC L-WN uncertainties, *Metrologia*, *51*(1), 40-47, doi: 10.1088/0026-1394/51/1/40.

Gleason, A. C. R., K. J. Voss, H. R. Gordon, M. Twardowski, J. Sullivan, C. Trees, A. Weidemann, J. F. Berthon, D. Clark and Z. P. Lee (2012), Detailed validation of the bidirectional effect in various Case I and Case II waters, *Optics Express*, *20*(7), 7630-7645, doi: 10.1364/oe.20.007630.

Goes, J. I., H. d. R. Gomes, E. M. Haugen, K. T. McKee, E. J. D'Sa, A. M. Chekalyuk, D. K. Stoecker, P. J. Stabeno, S.-I. Saitoh and R. N. Sambrotto (2014a), Fluorescence, pigment and microscopic characterization of Bering Sea phytoplankton community structure and photosynthetic competency in the presence of a Cold Pool during summer, *Deep Sea Research Part II: Topical Studies in Oceanography*, *109*(0), 84-99, doi: 10.1016/j.dsr2.2013.12.004.

Goes, J. I., H. d. R. Gomes, A. M. Chekalyuk, E. J. Carpenter, J. P. Montoya, V. J. Coles, P. L. Yager, W. M. Berelson, D. G. Capone, R. A. Foster, et al. (2014b), Influence of the Amazon River discharge on the biogeography of phytoplankton communities in the western tropical north Atlantic, *Progress In Oceanography*, *120*(0), 29-40, doi: 10.1016/j.pocean.2013.07.010.

Gomes, H. d. R., K. McKee and J. I. Goes (in prep), Improved methods for determination of phycoerythin and phycocyanin in natural seawater samples.
Gorbunov, M. Y. and P. G. Falkowski (2004), Fluorescence induction and relaxation (FIRe) technique and instrumentation for monitoring photosynthetic processes and primary production in aquatic ecosystems, *Proceedings of Photosynthesis: Fundamental Aspects to Global Perspectives"-Proc. 13th International Congress of Photosynthesis, Montreal, Aug*.
Gordon, H. R. (2010), Some reflections on thirty-five years of ocean-color remote sensing, in *Oceanography from Space: Revisited*, Edited by Barale, V., Gower, J.F.R. and Alberotanza, L., pp. 289-305, Springer Netherlands.
Gordon, H. R. and K. Ding (1992), Self-shading of in-water optical instruments, *Limnology and Oceanography*, *37*(3), 491-500.
Gordon, H. R. and M. Wang (1994), Retrieval of water-leaving radiance and aerosol optical thickness over the oceans with SeaWiFS: A preliminary algorithm, *Appl. Opt.*, *33*, 443–452.
Gordon, H. R., D. K. Clark, J. L. Mueller and W. A. Hovis (1980), Phytoplankton Pigments from the Nimbus-7 Coastal Zone Color Scanner: Comparisons with Surface Measurements, *Science*, *210*(4465), 63-66, doi: 10.2307/1684604.
Gould, R. W., R. A. Arnone and M. Sydor (2001), Absorption, scattering; and remote-sensing reflectance relationships in coastal waters: Testing a new inversion algorithm, *J. Coast. Res.*, *17*(2), 328-341.
Grum, F. and R. J. Becherer (1979), *Optical radiation measurements*, Academic Press.
GUM (1995), Evaluation of measurement data - Guide to the expression of uncertainty in measurement. http://www.bipm.org/en/publications/guides/gum.html.
Hedges, J. I. and J. H. Stern (1984), Carbon and nitrogen determinations of carbonate-containing solids, *Limnology and Oceanography*, *29*(3), 657-663, <Go to ISI>://WOS:A1984SX74500022.
Holm-Hansen, O. and B. Riemann (1978), Chlorophyll a determination: improvements in methodology, *Oikos*, *30*, 438-447.
Holm-Hansen, O., C. J. Lorenzen, R. W. Holmes and J. D. H. Strickland (1965), Fluorometric determination of chlorophyll, *Journal du Conseil*, *30*, 3-15.
Hooker, S. B. and G. Zibordi (2005), Platform perturbations in above-water radiometry, *Applied Optics*, *44*(4), 553-567, doi: 10.1364/ao.44.000553.
Hooker, S. B., S. McLean, M. Small, G. Lazin, G. Zibordi and J. Brown (2002), The Seventh SeaWiFS Intercalibration Round-Robin Experiment (SIRREX-7), March 1999. SeaWiFS Report NASA/TM-2001-206892, vol. 17, NASA Goddard Space Flight Center, Greenbelt, Maryland.
Hovis, W. A., D. K. Clark, F. Anderson, R. W. Austin, W. H. Wilson, E. T. Baker, D. Ball, H. R. Gordon, J. L. Mueller, S. Z. El-Sayed, et al. (1980), Nimbus-7 Coastal Zone Color Scanner: System Description and Initial Imagery, *Science*, *210*(4465), 60-63, doi: 10.2307/1684603.
Hunter, C. (2006), Particulate organic carbon, nitrogen and total suspended matter. Methodologies, protocols and analyses used in the development of ocean color product algorithms., Technical Publication 06–1, Moss Landing Marine Laboratories.
IOCCG (2010), Atmospheric correction for remotely-sensed ocean-colour products. Wang, M. (ed.), *Reports and monographs of the International Ocean-Colour Coordinating Group,* No. 10, International Ocean-Colour Coordinating Group, Dartmouth, Canada.
Johnson, B. C., J. Rice, H. Yoon and A. Parr (2014), Principles of optical radiometry, in *Optical radiometry for ocean climate measurements*, edited by Zibordi, G., Donlon, C. and Parr, A., pp. 13-67, Academic Press, Waltham, MA.
Kishino, M., M. Takahashi, N. Okami and S. Ichimura (1985), Estimation of the spectral absorption coefficients of phytoplankton in the sea, *Bulletin of Marine Science*, *37*(2), 634-642.
Lee, Z. P., N. Pahlevan, Y.-H. Ahn, S. Greb and D. O'Donnell (2013), Robust approach to directly measuring water-leaving radiance in the field, *Applied Optics*, *52*(8), 1693-1701.
Lee, Z. P., K. L. Carder, R. G. Steward, T. G. Peacock, C. O. Davis and J. L. Mueller (1997), *Remote-sensing reflectance and inherent optical properties of oceanic waters derived from above-water*

measurements, 160-166 pp., Spie - Int Soc Optical Engineering, Bellingham, doi: 10.1117/12.266436.

Leymarie, E., D. Doxaran and M. Babin (2010), Uncertainties associated to measurements of inherent optical properties in natural waters, *Applied Optics*, *49*(28), 5415-5436, doi: 10.1364/ao.49.005415.

MacIssac, E. A. and J. G. Stockner (1993), Enumeration of phototrophic picoplankton by autofluorescence microscopy., in *Handbook of Methodology in Aquatic Microbial Ecology*, Edited by Kemp.P.F., Sherr, B.F., Sherr, E.B. and J., C.J., pp. 187-197, Lewis Publishers, Boca Raton, Florida, USA.

Mannino, A., M. E. Russ and S. B. Hooker (2008), Algorithm development and validation for satellite-derived distributions of DOC and CDOM in the US Middle Atlantic Bight, *J. Geophys. Res.-Oceans*, *113*(C7), doi: 10.1029/2007jc004493.

Mitchell, B. G., M. Kahru, W. J. and S. M. (2003), Determination of spectral absorption coefficients of particles, dissolved material and phytoplankton for discrete water samples, in *Ocean Optics Protocols for Satellite Ocean Color Sensor Validation, NASA/TM-2003-211621/Rev4-Vol.IV*, Edited by Mueller, J.L., G.S., F. and J.L., M., pp. 39-64, NASA/Goddard Space Flight Center, Greenbelt, MD.

Mitchell, B. G., A. Bricaud, K. L. Carder, J. Cleveland, G. M. Ferrari, R. W. Gould, M. Kahru, M. Kishino, H. Maske, T. Moisan, et al. (2000), Determination of spectral absorption coefficients of particles, dissolved material and phytoplankton for discrete water samples, in *Ocean Optics Protocols for Satellite Ocean Color Sensor Validation, NASA/TM-2000-209966*, Edited by Fargion, G.S. and Mueller, J.L., pp. 125-153, NASA/Goddard Space Flight Center, Greenbelt, MD.

Mobley, C. D. (1999), Estimation of the remote-sensing reflectance from above-surface measurements, *Appl. Optics*, *38*(36), 7442-7455, doi: 10.1364/ao.38.007442.

Morel, A., D. Antoine and B. Gentili (2002), Bidirectional reflectance of oceanic waters: accounting for Raman emission and varying particle scattering phase function, *Applied Optics*, *41*(30), 6289-6306, doi: 10.1364/ao.41.006289.

Morrow, J. H., C. R. Booth, R. N. Lind and S. B. Hooker (2010), The Compact Optical Profiling System (C-OPS). Advances in Measuring the Apparent Optical Properties (AOPs) of Optically Complex Waters, NASA Tech. Memo. 2010–215856, 42–50 pp, NASA Goddard Space Flight Center, Greenbelt, Maryland.

Mueller, J. L., A. Morel, R. Frouin, C. Davis, R. Arnone, K. L. Carder, Z. P. Lee, R. G. Steward, S. Hooker, C. D. Mobley, et al. (2003), *NASA Tech. Memo. 2003-21621/Rev-Vol III*, Ocean optics protocols for satellite ocean color sensor validation, Revision 4. Ocean optics protocols for satellite ocean color sensor validation, NASA Goddard Space Flight Center, Greenbelt, Maryland.

Neckel, H. and D. Labs (1984), The solar radiation between 3300-A and 12500-A, *Solar Physics*, *90*(2), 205-258.

Ondrusek, M., E. Stengel, C. S. Kinkade, R. L. Vogel, P. Keegstra, C. Hunter and C. Kim (2012), The development of a new optical total suspended matter algorithm for the Chesapeake Bay, *Remote Sensing of Environment*, *119*, 243-254, doi: 10.1016/j.rse.2011.12.018.

Pegau, W. S., D. Gray and J. R. V. Zaneveld (1997), Absorption and attenuation of visible and near-infrared light in water: dependence on temperature and salinity, *Applied Optics*, *36*(24), 6035-6046, doi: 10.1364/ao.36.006035.

Pope, R. M. and E. S. Fry (1997), Absorption spectrum (380-700 nm) of pure water .2. Integrating cavity measurements, *Applied Optics*, *36*(33), 8710-8723, doi: 10.1364/ao.36.008710.

Porter, J. N., M. Miller, C. Pietras and C. Motell (2001), Ship-based sun photometer measurements using Microtops sun photometers, *J. Atmos. Ocean. Technol.*, *18*(5), 765-774, doi: 10.1175/1520-0426(2001)018<0765:sbspmu>2.0.co;2.

Richardson, T. L., E. Lawrenz, J. L. Pinckney, R. C. Guajardo, E. A. Walker, H. W. Paerl and H. L. MacIntyre (2010), Spectral fluorometric characterization of phytoplankton community composition using the Algae Online Analyser®, *Water Res*, *44*(8), 2461-2472.

Satlantic (2003), Operation Manual for Profiler II. Satlantic Incorporated, Halifax, Nova Scotia.

Satlantic (2004), SatView Data Logging / Display Program Users Guide; Version 2.8. Satlantic Incorporated, Halifax, Nova Scotia.

Sharp, J. H., C. A. Carlson, E. T. Peltzer, D. M. Castle-Ward, K. B. Savidge and K. R. Rinker (2002), Final dissolved organic carbon broad community intercalibration and preliminary use of DOC reference materials, *Marine Chemistry*, *77*(4), 239-253, doi: 10.1016/s0304-4203(02)00002-6.

Solar Light Company Inc (2003), Microtops II Sunphotometer user's guide, vers. 5.5. Philadelphia, PA.

Sullivan, J. M., M. S. Twardowski, J. R. V. Zaneveld, C. M. Moore, A. H. Barnard, P. L. Donaghay and B. Rhoades (2006), Hyperspectral temperature and salt dependencies of absorption by water and heavy water in the 400-750 nm spectral range, *Applied Optics*, *45*(21), 5294-5309.

Tomas, C. R. (1997), *Identifying marine phytoplankton*, Academic press.

Twardowski, M. S. and P. L. Donaghay (2001), Separating in situ and terrigenous sources of absorption by dissolved materials in coastal waters, *J. Geophys. Res.-Oceans*, *106*(C2), 2545-2560, doi: 10.1029/1999jc000039.

Twardowski, M. S., J. M. Sullivan, P. L. Donaghay and J. R. V. Zaneveld (1999), Microscale quantification of the absorption by dissolved and particulate material in coastal waters with an ac-9, *J. Atmos. Oceanic Technol.*, *16*, 691–707.

Van Heukelem, L. and C. S. Thomas (2001), Computer-assisted high-performance liquid chromatography method development with applications to the isolation and analysis of phytoplankton pigments, *Journal of Chromatography A*, *910*(1), 31-49, doi: 10.1016/s0378-4347(00)00603-4.

Voss, K. J. and G. Zibordi (1989), Radiometric and geometric calibration of a spectral electro-optic "fisheye' camera radiance distribution system, *J. Atmosph. and Ocean. Techn.*, *6*, 652-662.

Voss, K. J. and A. Morel (2005), Bidirectional reflectance function for oceanic waters with varying chlorophyll concentrations: Measurements versus predictions, *Limnology and Oceanography*, *50*(2), 698-705.

Voss, K. J. and A. L. Chapin (2005), Upwelling radiance distribution camera system, NURADS, *Optics Express*, *13*(11), 4250-4262, doi: 10.1364/opex.13.004250.

Voss, K. J., A. Morel and D. Antoine (2007), Detailed validation of the bidirectional effect in various Case 1 waters for application to ocean color imagery, *Biogeosciences*, *4*(5), 781-789.

Wang, M. (2007), Remote sensing of the ocean contributions from ultraviolet to near-infrared using the shortwave infrared bands: simulations, *Applied Optics*, *46*(9), 1535-1547, doi: 10.1364/ao.46.001535.

Wang, M., X. Liu, L. Tan, L. Jiang, S. Son, W. Shi, K. Rausch and K. Voss (2013), Impact of VIIRS SDR performance on ocean color products, *J. Geophys. Res. Atmos.*, *118*, 10347–10360, doi: doi:10.1002/jgrd.50793.

Wang, M., X. Liu, L. Jiang, S. Son, J. Sun, W. Shi, L. Tan, P. Naik, K. Mikelsons, X. Wang, et al. (2014), Evaluation of VIIRS Ocean Color Products, *Proc. SPIE 9261*, *92610E*, doi: 10.1117/12.2069251.

Welschmeyer, N. A. (1994), Fluorometric analysis of chlorophyll a in the presence of chlorophyll b and pheopigments, *Limnology and Oceanography*, *39*(8), 1985-1992.

WETLabs (2011), ac meter protocol document. ac meter protocol (acprot); Revision Q 20 April 2011.

Yoon, H. W. and C. E. Gibson (2011), Spectral irradiance calibrations, NIST Special Publications (U.S. Department of Commerce, Washington, D. C. 20402-9325, 2011), vol. *SP250-89*.

Zaneveld, J. R. V., J. C. Kitchen and C. C. Moore (1994), Scattering error correction of reflecting-tube absorption meters, *Proceedings*, doi: 10.1117/12.190095.

Zaneveld, J. R. V., E. Boss and A. Barnard (2001), Influence of surface waves on measured and modeled irradiance profiles, *Applied Optics*, *40*(9), 1442-1449, doi: 10.1364/ao.40.001442.

Zibordi, G. (2006), Immersion factor of in-water radiance sensors: Assessment for a class of radiometers, *J. Atmos. Ocean. Technol.*, *23*(2), 302-313, doi: 10.1175/jtech1847.1.

Zibordi, G. (2012), Comment on "Long Island Sound Coastal Observatory: assessment of above-water radiometric measurement uncertainties using collocated multi and hyperspectral systems", *Applied Optics*, *51*(17), 3888-3892, doi: 10.1364/ao.51.003888.

Zibordi, G. and G. M. Ferrari (1995), Instrument self-shading in underwater optical measurements: Experimental data, *Applied Optics*, *34*(15), 2750-2754.

Zibordi, G. and B. Bulgarelli (2007), Effects of cosine error in irradiance measurements from field ocean color radiometers, *Applied Optics*, *46*(22), 5529-5538, doi: 10.1364/ao.46.005529.

Zibordi, G. and K. J. Voss (2014), In situ Optical Radiometry in the Visible and Near Infrared, *Experimental Methods in the Physical Sciences*, *47*, 247-304.

Zibordi, G., D. D'Alimonte and J. F. Berthon (2004), An evaluation of depth resolution requirements for optical profiling in coastal waters, *J. Atmos. Ocean. Technol.*, *21*(7), 1059-1073, doi: 10.1175/1520-0426(2004)021<1059:aeodrr>2.0.co;2.

Zibordi, G., K. Ruddick, I. Ansko, G. Moore, S. Kratzer, J. Icely and A. Reinart (2012), In situ determination of the remote sensing reflectance: an inter-comparison, *Ocean Science*, *8*(4), 567-586, doi: 10.5194/os-8-567-2012.

Zibordi, G., B. Holben, I. Slutsker, D. Giles, D. D'Alimonte, F. Melin, J. F. Berthon, D. Vandemark, H. Feng, G. Schuster, et al. (2009), AERONET-OC: A Network for the Validation of Ocean Color Primary Products, *J. Atmos. Ocean. Technol.*, *26*(8), 1634-1651, doi: 10.1175/2009jtecho654.1.

Appendix A – Station Information Tables

Table A1. Station dates, start times, locations and descriptions

Station #	Day of Year	Date	Station Start* Time (UTC)	Station Start* Time (local)	Station Start* Latitude [decimal degrees]	Station Start* Longitude [decimal degrees]	Station Description and Comments
1	315	11-Nov	19:00	14:00	32.5418	79.4790	Charleston channel entrance; Coastal; Set up station
2	316	12-Nov	13:18	8:18	32.0884	78.3956	Offshore shelf
3	316	12-Nov	19:33	14:33	31.8835	78.1404	Stream front
4	317	13-Nov	12:49	4:49	32.6344	76.6293	In Gulf Stream
5	317	13-Nov	16:15	11:15	32.8703	76.7382	
6	317	13-Nov	18:48	13:48	33.1335	76.8279	Offshore front Stream; 3 nautical miles west of Gulf Stream temperature front
7	317	13-Nov	21:59	16:59	33.3997	76.9379	Offshore; Dark, overcast; Shingle, shedding of stream; West side of stream
8	318	14-Nov	17:05	12:05	34.6140	76.9910	Near coast (Morgan City); ac-9 calibration done in morning; Cold front passing
9	318	14-Nov	19:59	14:59	34.5281	76.8672	Coastal front; in sight of Cape Fear
10	319	15-Nov	13:00	8:00	34.9394	75.6985	Coastal; Long optics station
11	319	15-Nov	19:15	14:15	34.8718	75.4260	South of Hatteras; In Stream
12	320	16-Nov	13:31	8:31	35.3186	74.7214	Hatteras; Offshore; Stream; In Stream 4 knots north! Building seas
13	320	16-Nov	16:46	11:46	35.3459	74.8868	Short station at front, cross Stream north of Hatteras!
14	320	16-Nov	18:50	13:50	35.3883	75.0758	Hatteras; Coastal front; north of Hatteras
15	320	16-Nov	20:25	15:25	35.2486	75.1661	Optical thin layers! Moving down the coastal front off Hatteras
16	321	17-Nov	14:36	9:36	34.2192	77.1142	Some rain
17	322	18-Nov	13:46	8:46	33.5445	78.4768	Rough at night; winds to 30 kts, air temp 40°C
18	322	18-Nov	18:40	13:40	33.4101	78.5010	Saw particles in water
19	322	18-Nov	21:27	16:27	33.3299	78.4436	
20	323	19-Nov	14:02	9:02	32.0104	80.0773	
21	323	19-Nov	17:00	12:00	32.204	80.0704	Excellent conditions, clear skies, particles in water.
22	323	19-Nov	20:01	15:01	32.1811	79.9208	Heading east; Excellent sun; Last PM
23	324	20-Nov	13:01	8:01	32.5467	79.4894	End

*Station start data are representative of the conditions at the nominal "start" of the station. Station variability over time and space for the duration of the station are not quantified here but will be the subject of scientific analyses and future dissemination.

Table A2. Local deployment times of profiling radiometers, IOP packages and additional optical instruments

Station #	Profiling Radio-meters x4[1]	IOP Package (NASA/ GSFC)[2]	IOP Package (UMB)[3]	NURADS (U. Miami)	HyperPro Float (Stennis)	HyperPro SBA (UMB)	ASD x 6[4]	Spectral Evolution (UMB)	GER (CUNY)	Micro-Tops x 4[5]
	Local Time of Instrument Deployment									
1	14:30	14:46	12:40	n.d.	15:45	16:21	15:10	16:01	15:16	n.d.
2	12:00	10:59	8:20	9:30	10:30	11:04	10:00	11:58	10:23	10:10
3	14:45	15:59	15:30	n.d.	15:45	15:17	14:35	14:44	14:40	15:00
4	9:00	n.d.	8:00	n.d.	8:20	8:41	8:50	9:03	8:50	9:00
5	11:45	11:30	n.d.	n.d.	11:03	11:12	11:40	12:03	11:07	n.d.
6	14:39	13:38	13:55	14:39	13:40	14:07	14:15	14:28	14:46	n.d.
7	16:33	17:26	18:00	n.d.	16:40	17:12	16:30	n.d.	16:40	n.d.
8	12:55	12:19	n.d.	n.d.	13:05	n.d.	13:15	n.d.	12:38	n.d.
9	14:45	15:18	15:30	n.d.	15:00	15:08	14:50	n.d.	14:43	n.d.
10	9:15	8:43	8:57	10:45	8:29	8:28	9:27	9:37	9:55	08:00 09:00 10:00 11:00
11	13:15	20:01	14:30	13:55	13:55	14:09	13:55	13:18	13:41	12:30 13:00 14:00 15:00 16:00
12	10:02	8:42	8:56	n.d.	9:14	9:19	10:02	9:43	n.d.	08:00 09:00 10:00
13	11:50	n.d.	11:20	n.d.	n.d.	n.d.	11:25	n.d.	11:49	n.d.
14	13:28	14:05	13:45	n.d.	13:49	13:56	13:50	n.d.	13:39	n.d.
15	15:23	16:12	15:56	n.d.	n.d.	n.d.	n.d	n.d.	15:38	n.d.
16	9:40	8:43	8:50	n.d.	9:18	n.d.	8:40	n.d.	9:44	n.d.
17	10:05	9:32	9:45	n.d.	9:20	9:22	10:47	10:22	n.d.	09:00 10:00 11:00
18	13:28	12:41	12:25	14:30	12:31	12:44	13:15	n.d.	n.d.	12:00 13:00 14:00 15:00
19	16:00	16:57	17:30	n.d.	16:45	n.d.	16:10	n.d.	n.d.	16:00
20	10:08	9:36	9:47	n.d.	9:18	9:33	10:26	n.d.	10:20	n.d.
21	13:05	12:29	12:15	13:30	13:05	12:43	13:01	13:21	13:01	12:00 13:00 13:40
22	15:20	16:18	n.d.	15:53	15:53	15:58	15:23	n.d.	15:51	15:00 16:00
23	9:00	8:36	8:50	9:50	8:22	8:27	9:50	n.d.	10:15	08:00 09:30 10:30

[1]Two HyperPros (N OAA/STAR and USF); C-OPS (NASA/GSFC); MicroPro (JRC)
[2]NASA/GSFC IOP: ac-s, filtered ac-9, ECO BB9, VSF9, SBE 49
[3]UMB IOP: ac-s, filtered ac-s, BB7FL2, CTD
[4]ASD's: NOAA/STAR; USF and two from Stennis team (Naval Research Institue and University of Southern Mississippi)
[5]Microtops times are from Stennis deployments which has the most complete dataset. Four other Microtops were deployed at nominally similar times at various stations by NOAA/STAR, USF and CCNY.

Table A3. Bottom depth, local deployment times and bottle sampling depths of the ship's CTD Rosette package and sampling depths for measured parameters

Station #	Ocean Bottom Depth [m]	Local Time of CTD Profile	Chl-*a* and TSM (NOAA/ STAR)	HPLC Phytoplankton Pigments (NASA/GSFC)	POC, DOC, CDOM (NASA/GSFC)	Filter Pad Absorption and Chl-*a* (USF)	ALF, FIRe, bbe, Phycobili-pigments (LDEO)
			Sampling Depths [m]				
1	19.1	11:20	1	18, 1	18, 1	18, 1	18, 1
2	103	10:00	1	1	1	1	1
3	120	14:35	1	98, 35, 1	98, 35, 1	35, 1	98, 35, 1
4	2300	8:16	1	80, 32, 1	80, 32, 1	32, 1	80, 32, 1
5	2300	11:03	1	120, 39, 1	120, 39, 1	39, 1	120, 39, 1
6	121	14:20	1	100, 35, 1	35, 1	35, 1	100, 35, 1
7	151	17:10	1	96, 32, 1,	32, 1	32, 1	96, 32, 1
8	15.1	12:05	1	14, 6, 1	6, 1	6, 1	14, 6, 1
9	19.4	15:46	1	19, 10, 1	10, 1	10, 1	19, 10, 1
10	29.4	8:24	1	29, 12, 1	12, 1	12, 1	29, 12, 1
11	200	15:45	1	90, 35, 1	35, 1	35, 1	90, 35, 1
12	2187	8:15	1	90, 45, 1	45, 1	45, 1	90, 45, 1
13	400	11:39	1	70, 38, 1	38, 1	38, 1	70, 38, 1
14	32.5	13:45	1	26, 10, 1	10, 1	10, 1	26, 10, 1
15	28.7	16:23	1	11, 3, 1	11, 3	11, 3	11, 3, 1
16	27	8:23	1	27, 12, 1	12, 1	12, 1	27, 12, 1
17	18	9:15	1	15, 8, 2	8, 2	8, 2	15, 8, 2
18	22	15:10	1	20, 7, 1	7, 1	7, 1	20, 7, 1
19	26	16:30	1	26, 1	1	1	26, 1
20	23.1	9:18	1	21, 9, 1	9, 1	9, 1	21, 9, 1
21	17.9	12:43	1	17, 7, 1	7, 1	7, 1	17, 7, 1
22	26	16:02	1	25, 7.5, 1	7.5, 1	7.5, 1	25, 7.5, 1
23	19	8:20	1	17, 8, 1	8, 1	8, 1	17, 8, 1

Table A4. Environmental (wind, water, sky) conditions at the beginning of each station

Station #	Sky Cover (%)	Wind Direction [degrees]	Wind Speed [knots]	Sea State [ft]*	Sea Surface Temperature** [°C]	Sea Surface Salinity** [PSU]	Fluorescence** [uncalibrated voltage]	Absorption at 440 nm** [m^{-1}]
1	80	360	15	1-3	20.173	35.355	0.843	0.1556
2	15	330	10	2-4	26.874	36.356	0.271	0.0429
3	10	300	10	1-3	26.996	36.341	0.232	0.0415
4	10	315	3	1-2	26.876	36.371	0.284	0.0401
5	60	210	3	2-3	26.853	36.351	0.221	0.0402
6	100	210	7	1-2	25.413	35.987	0.516	0.0627
7	90	230	14	2-3	26.425	36.294	0.575	0.0509
8	100	350	15-20	2-3	18.171	35.287	1.292	0.4214
9	100	350	18	2-3	18.579	35.669	1.649	0.2299
10	30	0	16	3-4	21.044	34.962	0.728	0.137
11	40	340	17.5	2-3	23.285	36.122	0.601	0.0675
12	30	210	5	2-4	24.168	36.23	0.491	0.0585
13	100	195	17	2-4	23.507	36.16	0.524	0.062
14	95	175	12.5	1-2	16.958	32.881	1.146	0.1812
15	100	300	13	3	17.369	32.975	1.249	0.1713
16	80	165	17	3-5	19.892	36.07	0.302	0.0672
17	5	340	18.5	2-4	18.429	35.764	2.4822	0.4081
18	5	315	15	2-4	19.139	35.762	1.2131	0.2327
19	35	305	10	2-3	20.301	35.727	0.7095	0.0886
20	40	10	10.5	1-2	20.029	35.889	0.4078	0.0951
21	0	16	9	1	17.915	35.161	0.5039	0.1677
22	0	320	4	1	18.873	34.939	0.5113	0.1192
23	0	280	16	1-2	18.423	35.525	0.7559	0.1122

*These values are reported here in units of "feet" as they were recorded on the ship rather than converting them to SI units of m.
**The values for these parameters are taken from the underway flow-through system from instruments at the nominal "start" time of the station (see Table A-1).

Appendix B – Daily Station Summaries

A daily summary of stations and overnight transect locations and the criteria used for these locations are detailed below. Note that times are local (Eastern Standard Time, subtract 5 h for UTC). The conditions of percent cloud cover at the 23 stations are shown in Appendix A, Table A-4.

11 Nov. – Sampling started at the entrance to Charleston, SC at Station 1. This began at 1300L as preparation shakedown on instruments. There was only one station done for this day in order to get all instrument protocols operating.

At 1800L, we began an offshore line transect directly east across the Gulf Stream front using the flow-through instruments. Our overnight transect offshore cross the front and can back (westward) across the front to Station 2 for 12 Nov. morning.

12 Nov. – We began station 2 at 0800L on the west side of the Gulf Stream front. We moved to the East side of the Gulf Stream at Station 3 at 1300L. Cloud cover decreased from the previous day.

We departed Station 3 at 1800L for the overnight transect. This transect extended eastward to the east side of the Gulf Stream, and then northward following the Stream. We then began heading westward to the coast as a second Gulf Stream crossing. We arrived on the east side of the Gulf Stream front at 0800L the next morning.

13 Nov. – This day we had 4 stations crossing the front beginning at 0800L with Station 4 and separated by an hour transect of approximately 10 nautical miles. Stations 5 and 6 were at the frontal boundaries associated with coastal eddies and Gulf front shingles which were observed along the front in the satellite imagery. These stations will be representative of upwelling processes. Station 7 was on the west side of the front on shelf waters ending at 1700L. Cloud cover was variable throughout the day with conditions getting worse in late afternoon.

The overnight transect preceded westward toward the coast as the winds increased. We transected northward to arrive at Station 8 in the morning.

14 Nov. – Station 8 was in coastal waters began at 0800L offshore of Cape Lookout Shoals and to the north of the discharge of a small river from Swansboro. This region was protected by the strong winds offshore. We moved offshore northwestward to Station 9 in the afternoon across a coastal front. Conditions were overcast with increasing winds.

The overnight transect was designed to cross multiple coastal and shelf fronts that were observed in satellite imagery. The deteriorating weather conditions required us to remain close to the coast as we moved northward. Our transect required us to move offshore to round Cape Lookout Shoals (way point a) and then we returned close to the coast (way point b). We followed a zigzag pattern crossing the coastal waters fronts (way points c, d and e) and arriving at Station 10 in the morning.

15 Nov. – Station 9 began at 0800L and was located on 18 nautical miles south of Cape Hatteras in shelf waters. In the afternoon, we moved 15 nm southeastward to Station 10 which was located in the Gulf Stream waters. Weather conditions were improving as the winds were reduced.

We departed Station 10 and rode the Gulf Stream for approximately 50 nautical miles northward to just north of Cape Hatteras where the Gulf Stream separates from the coast and extends eastward.

16 Nov. – Today, we conducted a major crossing of the Gulf Stream with 4 stations. The crossing location that was selected represents a major Gulf Stream front with significant currents and variable water types. We began Station 12 at 0800L located in Gulf Stream waters which moved us northward (3 km) by the end of the station. Station 13 was located directly on the Gulf Stream front that was defined in the satellite imagery as a major change in chlorophyll and SST. The subsurface vertical properties confirmed the frontal structure. Station 14 was located on the shelf waters side of the front. As weather conditions were deteriorating, Station 15 was located southward of the transect, in shelf waters and closer to Cape Hatteras. Cloud cover increased during the day with increasing winds with the approach of a major cold front.

The deteriorating weather conditions required the cruise to begin a southerly transect back that would remain close to the protection of the coast. The overnight transect kept us offshore of Cape Hatteras and Cape Lookout in shelf waters with 6 foot seas with approach of the cold front.

17 Nov. – The location of Station 16, between Cape Lookout and Cape Fear in the coastal waters, was selected for protection from the strong cold front passage. The station was overcast but with patchy clouds as the cold front passed and conditions improved along the coast. Only one station was done on this day. The location of this station was at the end of the transect that we performed on 13 November.

The overnight transect headed southward by heading offshore around the shoals of Cape Fear and then westward toward the coast to get behind the cold front in clear skies and improved weather conditions.

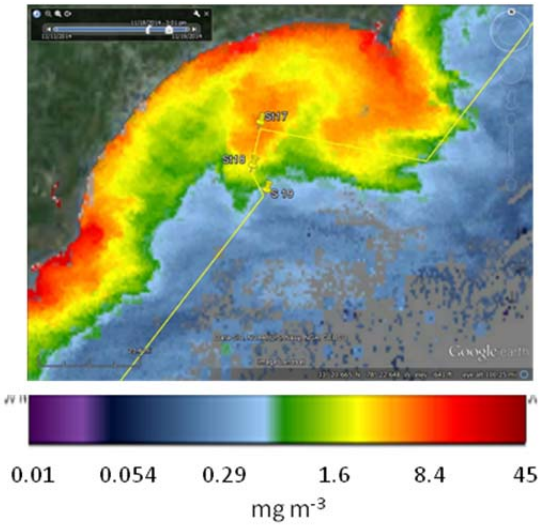

Figure B1. Locations of stations and cruise track from 18 November with the VIIRS-NRL chlorophyll imagery

18 Nov. – The passage of the front provided improving cloud cover conditions along the coast today. We selected some different water masses to sample based on the satellite imagery. Three stations (17, 18 and 19) were collected across different coastal and shelf waters. Station 17 began at 0800L in coastal waters approximately 20 nautical miles east of Myrtle Beach in approximately 70 m water depth. The three stations represent a transect of a phytoplankton bloom that originated offshore and extended southward. The bloom is clearly shown in the 18 and 19 November imagery. Station 17 was located in elevated chlorophyll. Station 18 was 9 nautical miles directly southward at a reduced chlorophyll concentration and Station 19 was 6 nautical miles south eastward on the other side of the bloom front with open water conditions. These 3 stations identify different water types across a coastal bloom formation and dissipation as is shown in the imagery with reduced cloud cover. Conditions were substantially

improved with the passage of the cold front for the remainder of the cruise! The locations of the stations in the phytoplankton bloom are shown in Figure B1.

The overnight transect on 18 November headed 110 nautical miles southward in shelf waters. The transect then turned west to arrive at station 20 at 0800L.

19 Nov. – Three stations (20, 21 and 22) were collected in cloud free conditions south of the Charleston, SC entrance in shelf waters. These waters represent 3 different water masses from offshore across the shelf front. This region had excellent sky conditions with good matchups between satellite and measurements (Fig. B2).

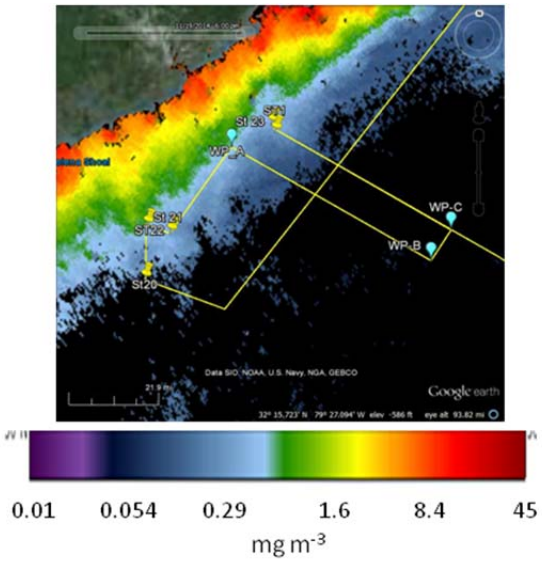

Figure B2. Locations of Stations 20, 21 and 22 on 19 November showing the transect of the shelf fronts with respect to chlorophyll image.

The night transect for 19 November sampled the Gulf Stream waters by two parallel crossings. Upon leaving Station 22 at 1800L, the ship proceeded northeastward to way point a, the coastal end of the transect. The ship than transected eastward ending at way point b and transected the Gulf Stream front. The ship next proceeded on a return transect westward from way point c to Station 23, our final station (see Fig. B2). This westward return transect was parallel to the offshore transect by 7.3 nautical miles. These cruise tracks will be examined for the changes in the water properties from these two Gulf Stream crossings by using the underway flow-through data.

20 Nov. – Station 23 was located at the entrance to Charleston Harbor at the same location as Station 1 that was sampled on 11 November. The station collection began at 0900L and ended at 1300L when we headed into port. Weather conditions were excellent with minimal cloud cover.

Appendix C – **Abbreviations, Units and Acronyms**

Table C1. Notations, descriptions and units if applicable

Abbreviation	Description	Typical Units (if applicable)
0^-	Just below water surface	
A	Reflectance factor for white target	
a	Absorption	m^{-1}
$a(715)$	Absorption at wavelength 715 nm	m^{-1}
$a(\lambda)$	Spectral absorption	m^{-1}
$a^*_{ph}(\lambda)$	Spectral chlorophyll-specific phytoplankton absorption	m^{-1}
a_{CDOM}	Absorption due to CDOM	m^{-1}
$a_d(\boldsymbol{\lambda})$	Spectral absorption of detrital matter	m^{-1}
AERONET	Aerosol Robotic Network (NASA)	
a_g	Absorption due to gelbstoff (detrital matter)	m^{-1}
AOPs	Apparent optical properties	
AOT	Aerosol optical thickness	
a_p	Absorption due to particles	m^{-1}
$a_p(\lambda)$	Spectral absorption due to particles	m^{-1}
a_{pg}	Absorption due to particles plus gelbstoff (detrital matter)	m^{-1}
a_t	Total absorption (all components)	m^{-1}
$A_{(t-w)}$	Total absorption minus absorption of pure water	m^{-1}
b	Scattering (in any/all directions)	m^{-1}
b_b	Backscattering (scattering in the backwards direction)	m^{-1}
BRDF	Bi-directional reflectance distribution function	
$b(\lambda)$	Spectral scattering	m^{-1}
c	Attenuation	m^{-1}
$C_{\Im}(\lambda)$	spectral in–air absolute calibration coefficient (i.e., absolute responsivity)	
Cal/Val	Calibration and Validation	
CCNY	City College of New York	
CDOM	Chromophoric dissolved organic material	ppb
$C_E(\lambda)$	Absolute spectral radiometric calibration coefficient for irradiance	mW cm^{-2} μm^{-1} $counts^{-1}$
c_g	Attenuation due to gelbsoff (detrital matter)	
Chl	Chlorophyll pigments	mg m^{-3}
Chl-*a*	Chlorophyll *a*	mg m^{-3}
C	un-calibrated data read from instrument	
$C_L(\lambda)$	In–air absolute spectral calibration coefficient for radiance	mW cm^{-2} μm^{-1} sr^{-1} $counts^{-1}$
CLASS	Comprehensive Large Array-data Stewardship System	
c_t	Total attenuation	m^{-1}
$c_t(\lambda)$	Spectral total attenuation	m^{-1}
CZCS	Coastal Zone Color Scanner instrument aboard the NIMBUS-7 satellite	
d	Distance between source and sensor	m
d_0	Distance at which the value E0(λ) was determined	m
$D0(\lambda)$	Dark value	
$DA(\Im(\lambda)$	Ambient light	
$DN(\Im(\lambda))$	Digital output corrected for the ambient light	
$DN(\Im(\lambda))^*$	Actual digital output	
$DN(E(\lambda))$	Digital output of spectral irradiance	
DOC	Dissolved Organic Carbon	mmol C m^{-3}
E	Irradiance	mW cm^{-2} μm^{-1}
$E(\lambda)$	Spectral irradiance	mW cm^{-2} μm^{-1}
$E_0(\lambda)$	Spectral irradiance of a specified source	mW cm^{-2} μm^{-1}
E_d	Downwelling irradiance	mW cm^{-2} μm^{-1}
$E_d(0^-, \lambda, t_0)$	Spectral downwelling irradiance just below surface at time $t = 0$	mW cm^{-2} μm^{-1}
$E_d(0^+, \lambda)$	Spectral downwelling irradiance just above surface	mW cm^{-2} μm^{-1}
$E_d(0^+, \lambda, t)$	Spectral downwelling irradiance just above surface at time t	mW cm^{-2} μm^{-1}
$E_d(0^+, \lambda, t_0)$	Spectral downwelling irradiance just above surface at time $t = 0$	mW cm^{-2} μm^{-1}
$E_d(z, \lambda, t)$	Spectral downwelling irradiance at depth z at time t	mW cm^{-2} μm^{-1}
$E_d(\boldsymbol{\lambda})$	Spectral downwelling irradiance	mW cm^{-2} μm^{-1}
EDIS	Environmental Data Information Service	
EDR	Environmental Data Record	
EDS	Environmental Data Service	
EPA	US Environmental Protection Agency	
E_s	Downwelling irradiance just above water surface	
$E_s(\boldsymbol{\lambda})$	Spectral downwelling irradiance just above water surface	
ESSA	Environmental Science Services Administration	
E_u	Upwelling irradiance	mW cm^{-2} μm^{-1}
$E_u(0^-, \lambda, t_0)$	Spectral upwelling irradiance just below water surface at time $t = 0$	mW cm^{-2} μm^{-1}

$E_u(z, \lambda, t)$	Spectral upwelling irradiance at depth z at time t	mW cm^{-2} µm^{-1}
$E_u(z, \lambda, t_0)$	Spectral upwelling irradiance at depth z at time $t = 0$	mW cm^{-2} µm^{-1}
FAFOV	Full Angle Field of View	
FEL	Lamp type designation assigned by the American National Standards Institute (not an acronym)	
F_L	Unknown spectral response calibration factor	
$\boldsymbol{F_0}$	Mean extraterrestrial solar irradiance	mW cm^{-2} µm^{-1}
FOV	Field of view	
Fv/Fm	Variable fluorescence	
FWHM	Full width half maximum	
HPLC	High Pressure Liquid Chromatography	
$I_f(\lambda)$	Spectral immersion factor accounting for the change in responsivity of the sensor when immersed in water with respect to air	
I_i	integration time used for that reading	s
I_N	normalized integration time	s
IOCCG	International Ocean Colour Coordinating Group	
IOPs	Inherent optical properties	
JPSS	Joint Polar Satellite System (program)	
JPSS-1	Joint Polar Satellite System -1 (satellite)	
JRC	Joint Research Centre (of the European Commission)	
$K_{\Im}(z_1, z_2, \lambda, t_0)$	Spectral downwelling diffuse attenuation coefficient between depths z= 1 and z=2 at time $t = 0$	m^{-1}
K_d	Downwelling diffuse attenuation coefficient	m^{-1}
$K_d(z_1, z_2, \lambda, t_0)$	Spectral downwelling diffuse attenuation coefficient between depths z= 1 and z=2 at time $t = 0$	m^{-1}
$K_l(\lambda)$	Spectral upwelling attenuation coefficient	m^{-1}
K_{Lu}	Upwelling radiance diffuse attenuation coefficient	m^{-1}
$K_u(z_1, z_2, \lambda, t_0)$	Spectral upwelling diffuse attenuation coefficient between depths z= 1 and z=2 at time $t = 0$	m^{-1}
L	Radiance	mW cm^{-2} µm^{-1} sr^{-1}
$L(\lambda)$	Spectral radiance	mW cm^{-2} µm^{-1} sr^{-1}
L_d	Downwelling radiance	mW cm^{-2} µm^{-1} sr^{-1}
LDEO	Lamont-Doherty Earth Observatory at Columbia University	
L_i	Sky radiance	mW cm^{-2} µm^{-1} sr^{-1}
$L_i(\theta', \Delta\phi, \lambda)$	Spectral sky radiance at given viewing geometry	mW cm^{-2} µm^{-1} sr^{-1}
LISCO	Long Island Sound Coastal Observatory	
L_{ref}	Radiance of reference	mW cm^{-2} µm^{-1} sr^{-1}
L_{sky}	Radiance of sky	mW cm^{-2} µm^{-1} sr^{-1}
L_t	Total radiance	mW cm^{-2} µm^{-1} sr^{-1}
$L_T(\theta, \Delta\phi, \lambda)$	Spectral total radiance at given viewing geometry	mW cm^{-2} µm^{-1} sr^{-1}
L_u	Upwelling radiance	mW cm^{-2} µm^{-1} sr^{-1}
$L_u(0^-, \lambda, t_0)$	Spectral upwelling radiance just below water surface and at time $t = 0$	mW cm^{-2} µm^{-1} sr^{-1}
$L_u(z, \lambda, t)$	Spectral upwelling radiance at depth z and time t	mW cm^{-2} µm^{-1} sr^{-1}
$L_u(z, \lambda, t_0)$	Spectral upwelling radiance at depth z at time $t = 0$	mW cm^{-2} µm^{-1} sr^{-1}
L_w	Water-leaving radiance	mW cm^{-2} µm^{-1} sr^{-1}
$L_w(0^+)$	Water-leaving radiance just above the surface	mW cm^{-2} µm^{-1} sr^{-1}
MIN	Minimum	
MOBY	Marine Optical BuoY	
MODIS	NASA's Moderate Resolution Imaging Spectroradiometer	
n	number of readings	
n.d.	Not determined	
NASA	National Aeronautics and Space Agency	
NASA/GSFC	NASA/Goddard Space Flight Center	
NCEI	National Centers for Environmental Information	
NESC	National Environmental Satellite Center	
NESDIS	National Environmental Satellite, Data, and Information Service	
NESS	National Environmental Satellite Service	
NIR	Near infrared	
NIST	National Institute of Standards and Technology	
$nL_w(\lambda)$	Spectral normalized water-leaving radiance	
NOAA	National Oceanic and Atmospheric Administration	
NOAA/STAR	NOAA/Center for Science tech, algorithm, research	
NRL	Naval Research Laboratory	
$n_w(\lambda)$	Refractive index of seawater	
OMAO	Office of Marine and Air Operations	
PAR	Photosynthetically Active Radiation	
PE-1, PE-2, PE-3	Phycoeurythrins groups 1, 2 and 3	
PN	Particulate Nitrogen	mmol N m^{-3}
POC	Particulate Organic Carbon	mmol C m^{-3}
PSII	Photosystem II	

PSU	Practical salinity unit	
PUB/PEB	phycourobilin/phycoerythrobilin	
Q_n	Q-factor at nadir	sr
$r(\lambda)$	diffuse to direct irradiance ratio	
RFU	Relative fluorescence units	
R_g	Bi-directional reflectance of grey card	
R_{rs}	Remote sensing reflectance	sr^{-1}
$R_{rs}(698, t)$	Remote sensing reflectance at wavelength of 698 nm at time t	sr^{-1}
$R_{rs}(\lambda)$	Spectral remote sensing reflectance	sr^{-1}
R_{tile}	Relative reflectance of blue tile	
S	Radiometric spectrum measurement	
SABOR	Ship-Aircraft Bio-Optical Research	
SeaWiFs	Sea-viewing Wide Field-of-view Sensor	
S_g	Radiometric spectrum measurement of grey card	
SNPP	Suomi National Polar-orbiting Partnership	
S_{sfc}	Radiometric spectrum measurement of surface water	
S_{sky}	Radiometric spectrum measurement of sky	
SST	Sea surface temperature	°C
S_{tile}	Radiometric spectrum measurement of blue tile	
t	Time	s
TSM	Total suspended matter	$mg\ L^{-1}$
U. Miami	University of Miami	
UMB	University of Massachusetts – Boston	
USF	University of South Florida	
USM	University of Southern Mississippi	
UTC	Universal Time Constant	
UTC	Coordinated Universal Time	
UV	Ultraviolet	
VIIRS	Visible Infrared Imaging Radiometer Suite	
z	Water depth	m
$\Delta\phi$	Relative azimuth between the sun and the instrument viewing direction	°
λ	Wavelength	nm
φ	Relative azimuth of the sensor to the sun	°
ρ	Reflectance	
$\rho(\lambda, \theta)$	Fresnel reflectance factor of seawater	
$\rho_d(\lambda, 0, \theta)$	Directional–directional reflectance	
$\rho_h(\lambda, \theta)$	Directional–hemispherical reflectance	
σPSII	Functional cross section of photosystem II	Å
θ	Angle	°
θ_g	Sensor zenith angle for grey card	°
θ_{sfc}	Sensor zenith angle for water surface	°
θ_{sky}	Sensor zenith angle for sky	°
$\aleph(\lambda)$	Spectral correction factor of system performance	
$\Im_0(0^-, \lambda, t_0)$	Reduced spectral free-fall radiometric data just below the surface water at time $t = 0$	
$\Im(\lambda)$	Reduced spectral free-fall radiometric data	
$\Im(z, \lambda, t)$	Reduced spectral free-fall radiometric data at depth z and time t	

Table C2. Instrument shorthand, description and manufacturer with modifications when applicable.

Instrument Shorthand	Full Identification/Purpose	Manufacturer or Citation
ac-9	In situ spectrophotometer - 9 channel resolution	WET Labs
ac-s	In situ spectrophotometer – high spectral resolution	WET Labs
ADCP	Acoustic Doppler Current Profiler	Teledyne RD Instruments
ALF	Advanced Laser Fluorometer	WET Labs
ASD	Analytical Spectral Device; HandHeld2-Pro visible and near infrared spectrophotometer	PANalytical
ECO BB3	Backscatter – 3 channels	WET Labs
BB7FL2	Backscatter – 7 channels, Fluorescence – 2 channels	WET Labs
ECO BB9	Backscatter – 9 channels	WET Labs
C-OPS	compact hyperspectral optical profiling system	Biospherical Instruments, Inc.
CTD	Conductivity, Temperature, Depth	Generic, various manufacturers
ECO Puck Triplet Fluorometer	Fluorescence at 3 channels for determining chlorophyll, CDOM and phycoerythrin	WET Labs
ECO Puck Triplet Scatterometer	Scatter – 3 channels (443, 550, 860)	WET Labs
FRRF	Fast Repetition Rate Fluorometer	Generic
GER	Field portable spectroradiometer	Spectra Vista Corporation
FlowCam	Dynamic imaging particle analysis for species composition and size measurements	Fluid Imaging Technologies, Inc.
HyperOCI	Hyperspectral irradiance sensor	Satlantic
HyperOCR	Hyperspectral radiance sensor	Satlantic
HyperPro	Free-falling hyperspectral optical profiler	Satlantic
HyperSAS	Above water optical system	Satlantic
HyperSAS-POL	Above water optical system with sky polarimeter	Satlantic with modifications by CCNY
HyperTSRB	Hyperspectral radiometer configured to float on the sea surface	Satlantic
MicroPro	Free-falling multispectral optical profiler	Satlantic
Microtops	Hand-held sun photometer (atmospheric aerosols and optical depth)	Solar Light Company
Mini-FIRe	Variable fluorescence	Satlantic
NURADS	Upwelling Radiance Distribution Camera System	Voss and Chapin, 2005
Sartorius CPA 2250	Balance	Sartorius
SBA	Sky Blocking Approach	Lee et al. 2013
SBE 49	Conductivity, Temperature, Depth	SeaBird
TRIoS	Above water hyperspectral radiometry package	TriOS GmbH
VSF-9	Volume scattering function – 9 channels	WET Labs
AlgaeOnlineAnalyser	Spectral fluorometer	bbe Moldeanke
SR1900	Spectroradiometer	Spectral Evolution, Inc.